Journal of Nonlinear Waves (2026), **2**, e16, 1–42
doi:10.1017/jnw.2026.10042

CAMBRIDGE UNIVERSITY PRESS

RESEARCH ARTICLE

Whitham modulation equations for the regularized Boussinesq equation with cubic nonlinearity

Mark A. Hoefer[1] and Anna Vainchtein[2]

[1]Department of Applied Mathematics, University of Colorado Boulder, Boulder, CO, USA
[2]Department of Mathematics, University of Pittsburgh, Pittsburgh, PA, USA
Corresponding author: Anna Vainchtein; Email: aav4@pitt.edu

Keywords: convexity; periodic travelling waves; Whitham modulation equations

(Received 30 March 2026 UTC; revised 16 June 2026 UTC; accepted 18 June 2026 UTC)

Abstract
A regularized Boussinesq equation is studied as a dispersive, long-wave (quasicontinuum) approximation of the Fermi–Pasta–Ulam lattice with a general cubic interaction force. Explicit periodic travelling wave solutions in terms of Jacobi elliptic functions are classified, and their solitary-wave, kink and trigonometric limits are obtained. The Whitham modulation equations describing slow modulations of periodic travelling wave solutions are derived using an averaged variational principle. The convexity (strict hyperbolicity, genuine nonlinearity) of the resulting hydrodynamic-type equations is examined numerically in general and analytically in the solitary-wave and harmonic limits. In particular, the loss of hyperbolicity and the formation of complex conjugate characteristic velocities is shown to lead to modulational instability of periodic travelling waves. The onset of modulational instability is verified by numerical computations of linearized spectra for periodic travelling waves and initial value problems that also reveal additional short-wavelength instabilities.

1. Introduction

Nonlinear waves in non-integrable Hamiltonian lattices, such as the celebrated Fermi–Pasta–Ulam (FPU) problem [18] and its various extensions and physical applications, have attracted a lot of attention [7, 20, 27, 31, 34, 38]. The dynamics of these waves is very rich due to the combination of higher order dispersion intrinsic to the lattice setting and higher order nonlinearity that is often present in such models. In the absence of integrability, this combination makes the tools of Whitham modulation theory and more recent advances in dispersive hydrodynamics [16, 25, 39] particularly promising for providing insight into the collective, multiscale dynamics of interacting lattice waves and for describing complex waveforms such as dispersive shock waves and travelling waves connecting periodic orbits. Some work in this direction has begun [11–13, 19, 35, 40] but much remains to be investigated.

A fundamental concept of primary importance for lattice dispersive hydrodynamics is the hyperbolicity of the modulation equations for the FPU problem. Hyperbolicity governs the dynamical stability and structure of multiscale wave dynamics [39]. In the non-integrable FPU problem, hyperbolicity has only been assessed in some special limits, such as the harmonic chain, the hard-sphere model and small-amplitude periodic travelling waves [12]. Another related concept for a hyperbolic system is that of a genuinely nonlinear characteristic field [29], which is a necessary condition for the construction of simple waves (integral curves) that form the foundation for solutions to Riemann problems and dispersive shock waves [16]. We say that a hydrodynamic-type system of Whitham modulation equations is

© The Author(s), 2026. Published by Cambridge University Press. This is an Open Access article, distributed under the terms of the Creative Commons Attribution licence (http://creativecommons.org/licenses/by/4.0), which permits unrestricted re-use, distribution and reproduction, provided the original article is properly cited.

Downloaded from https://www.cambridge.org/core. 16 Nov 2026 at 15:29:29, subject to the Cambridge Core terms of use.

convex if it is strictly hyperbolic and genuinely nonlinear [30]. A modulation system may be convex for a restricted subset of the state variables.

The present work focuses on studying the modulation system and its convexity for the modified regularized Boussinesq equation, a non-integrable dispersive partial differential equation that approximates FPU dynamics [33]. The regularized Boussinesq equation has been shown to capture some FPU features, including travelling kink fronts, solitary waves and dispersive shocks [36, 40]. We consider a general cubic nonlinearity that enables construction of explicit periodic travelling waves in terms of elliptic functions and systematically investigate all of the different cases and special limits. While it is typically assumed that all of the roots of the polynomial determining periodic travelling waves are real, our analysis includes the case when two of the roots become complex, which is relevant for the nonlinear interaction force with positive cubic-term coefficient. The transition from real to complex roots involves a bifurcation where the solution is a trigonometric wave. We then proceed to derive the Whitham modulation equations using Whitham's averaged variational principle [25, 39] and discuss their structure for three distinct cases: i) quadratic nonlinearity $w + w^2$ and cubic nonlinearities ii) $w + w^3$, iii) $w - w^3$. The cubic cases correspond to a nonconvex hyperbolic flux. We also discuss the reduction of these equations in the harmonic and solitary-wave limits. In the case of $w - w^3$, we obtain the wave-action conservation law for the kink limit, which yields a non-classical, undercompressive shock [17, 23], or superkink [22].

The main part of the paper focuses on determining the regions of convexity for the Whitham system where it is strictly hyperbolic and genuinely nonlinear. In the harmonic and solitary-wave limits, the convexity is examined analytically, and the full Whitham system is studied numerically. In each case, we identify parameterizations that allow us to present the results in a systematic way in terms of physically relevant parameters. In the case of quadratic nonlinearity, a symmetry of the governing equations enables a complete convexity characterization of the modulation system in terms of a two-dimensional parameter space. Meanwhile, in the cubic cases, a three-dimensional parameterization is needed, and we convey the results in a two-parameter plane for different values of the wave amplitude. The regions where hyperbolicity fails are indicated by contour plots of the imaginary part of the corresponding eigenvalue, while the loss of genuine nonlinearity is indicated by curves in the two-dimensional parameter plane.

Our results show that in the case of quadratic nonlinearity, the Whitham system is convex, i.e., strictly hyperbolic and genuinely nonlinear, for sufficiently small amplitude and sufficiently large mean strain. In the real-root case for nonlinearity $w + w^3$, our computations suggest strict hyperbolicity of the Whitham equations in the entire parameter range. However, the system loses genuine nonlinearity along two curves that bifurcate from the solitary-wave limit. The situation is different in the complex-root case, where we observe loss of hyperbolicity in an amplitude-dependent part of the parameter domain, as well as loss of genuine nonlinearity in up to three characteristic fields. As the amplitude is increased, the convexity domain becomes larger. In the case of cubic nonlinearity $w - w^3$, the convexity figures become even more complex. For a fixed amplitude, there are two domains where hyperbolicity is lost, including a parameter range in the solitary-wave limit, in addition to several curves marking the loss of genuine nonlinearity. The convexity domain is larger for smaller amplitudes in this case.

The loss of hyperbolicity is known to correspond to modulational instability [39], and rigorously so in some specific cases [1, 3, 8, 24]. We verify the onset of modulational instability by numerically computing the spectrum of the linearized operator using the Floquet–Fourier–Hill method [10] and show that the slopes of the associated cross structure in the spectrum near the origin are well approximated in terms of the real and imaginary parts of the Whitham characteristic velocities. In addition to confirming the emergence of modulational instability, our spectral calculations reveal short-wavelength instabilities in both modulationally stable and unstable cases, including superharmonic instabilities studied in detail in [2] for the case of quadratic nonlinearity. We also conduct numerical simulations initiated by modulationally unstable periodic travelling waves perturbed by the corresponding unstable eigenmode. The results confirm the development of modulational instability along with short-wavelength instabilities that eventually lead to the blowup of the solution in some cases.

Downloaded from https://www.cambridge.org/core. 16 Nov 2026 at 15:29:29, subject to the Cambridge Core terms of use.

The rest of the paper is organized as follows. In Section 2, we introduce the quasicontinuum model and discuss parameter reduction, conservation laws and averaging. Explicit periodic travelling wave solutions, their harmonic, solitary-wave and kink limits, existence domain and parameterizations are discussed in Section 3. In Section 4, we derive the Whitham modulation equations and investigate their structure, special limits and convexity. In Section 5, we verify the onset of modulational instability and explore other instability modes by examining the spectra of the linearized operator and conducting numerical simulations. Concluding remarks are found in Section 6.

2. Preliminaries

2.1. *Quasicontinuum model*

We consider the dispersive quasicontinuum model (modified regularized Boussinesq equation)

$$u_{tt} - \frac{1}{12}u_{xxtt} = (f(u_x))_x, \tag{2.1}$$

which approximates the FPU problem

$$\ddot{u}_n = f(u_{n+1} - u_n) - f(u_n - u_{n-1}) \tag{2.2}$$

for a chain of masses with displacements $u_n(t)$ and interaction force $f(w)$. This can be shown [33] by rewriting (2.2) in terms of strain variables $w_n = u_n - u_{n-1}$, using a Padé approximation of the discrete operator and integrating the resulting PDE to obtain the displacement formulation (2.1). In what follows, we consider the cubic interaction force

$$f(w) = w + \alpha w^2 + \beta w^3, \tag{2.3}$$

which corresponds to the α-β-FPU problem (2.2).

Observe that if $\beta > \alpha^2/3$ or $\beta < 0$, the change of variables

$$u(x,t) = \left(1 - \frac{\alpha^2}{3\beta}\right)^{1/2} y(x,\tau) - \frac{\alpha}{3\beta}x, \quad \tau = \left(1 - \frac{\alpha^2}{3\beta}\right)^{1/2} t,$$

yields the reduced equation

$$y_{\tau\tau} - y_{xx} - \beta\left(y_x^3\right)_x - \frac{1}{12}y_{xx\tau\tau} = 0$$

that involves no quadratic term in the interaction force. Because of this, we can, in the aforementioned regimes, set $\alpha = 0$. The additional rescaling $\sqrt{|\beta|}y \to y$ allows one to take $\beta = \pm 1$ without loss of generality. Similarly, if $\beta = 0$ but α is nonzero (quadratic interaction), the rescaling $\alpha u \to u$ means that we can set $\alpha = 1$. This change of variables is reminiscent of the transformation of solutions of the Gardner equation to solutions of the modified Korteweg-de Vries or Korteweg-de Vries equations [26]. In what follows, we will proceed with $\alpha, \beta \in \mathbb{R}$ and either $\beta > \alpha^2/3$, $\beta < 0$, or $\beta = 0$ and then restrict to $\alpha = 0$, $\beta = \pm 1$ and $\alpha = 1$, $\beta = 0$ when convenient.

Linearizing (2.1) about the uniformly deformed state by setting $u(x,t) = x\overline{w} + \epsilon e^{i(kx-\omega_0 t)}$ and taking the limit $\epsilon \to 0$, we obtain the linear dispersion relation

$$\omega_0^2(k,\overline{w}) = \frac{k^2 c_s^2(\overline{w})}{1 + k^2/12} < 12c_s^2(\overline{w}), \tag{2.4}$$

Downloaded from https://www.cambridge.org/core. 16 Nov 2026 at 15:29:29, subject to the Cambridge Core terms of use.

where

$$c_s(\overline{w}) = (f'(\overline{w}))^{1/2} = (1 + 2\alpha\overline{w} + 3\beta\overline{w}^2)^{1/2} \tag{2.5}$$

is the sound (long-wave) speed.

2.2. *Conservation laws*

Equation (2.1) corresponds to the Lagrangian density

$$\mathbb{L} = \frac{1}{2}v^2 - \phi(w) + \frac{1}{24}w_t^2, \tag{2.6}$$

where $w = u_x$ is the strain, $\phi(w)$ is the elastic energy density determining the force $f(w) = \phi'(w)$, and $v = u_t$ is the particle velocity. The regularized Boussinesq equation (2.1) can be written as the first-order system in conservative form

$$w_t - v_x = 0, \quad v_t - \left(f(w) + \frac{1}{12}w_{tt}\right)_x = 0. \tag{2.7}$$

Translational invariance of $\mathbb{L}$ implies two additional conservation laws that are equivalent for smooth solutions [21]. The first one is the energy balance,

$$\frac{\partial}{\partial t}\left(\phi(w) + \frac{v^2}{2} + \frac{1}{24}w_t^2\right) - \frac{\partial}{\partial x}\left[\left(f(w) + \frac{1}{12}w_{tt}\right)v\right] = 0, \tag{2.8}$$

where $\phi(w) + \frac{v^2}{2} + \frac{1}{24}w_t^2$ is the energy density, and $-(f(w) + \frac{1}{12}w_{tt})v$ is the energy flux. The second (Bernoulli–Eshelby) conservation law is

$$\frac{\partial}{\partial t}\left(wv + \frac{1}{12}w_x w_t\right) - \frac{\partial}{\partial x}\left(wf(w) + \frac{1}{12}ww_{tt} + \frac{1}{2}v^2 - \phi(w) + \frac{1}{24}w_t^2\right) = 0, \tag{2.9}$$

where $wv + \frac{1}{12}w_x w_t$ is the momentum density, and $\phi(w) - wf(w) - \frac{1}{24}w_t^2 - \frac{1}{2}v^2 - \frac{1}{12}ww_{tt}$ is the momentum flux.

2.3. *Averaged conservation laws*

As shown in Section 3, under certain conditions, there exists a four-parameter family of periodic travelling wave solutions

$$w = w(\theta; \mathbf{r}), \quad v = v(\theta; \mathbf{r}), \tag{2.10}$$

of (2.7) with modulated phase

$$\theta = S(X,T)/\epsilon, \quad \theta_x = S_X = k(X,T), \quad \theta_t = S_T = -\omega(X,T),$$

and parameters $\mathbf{r} = (r_1, r_2, r_3, r_4)$ that are allowed to vary on slow spatio-temporal scales $X = \epsilon x$, $T = \epsilon t$, $0 < \epsilon \ll 1$: $\mathbf{r} = \mathbf{r}(X,T)$. The nonlinear dispersion relation yields $k(X,T) = k(\mathbf{r}(X,T))$,

Downloaded from https://www.cambridge.org/core. 16 Nov 2026 at 15:29:29, subject to the Cambridge Core terms of use.

$\omega(X,T) = \omega(\mathbf{r}(X,T))$. We can formally obtain the Whitham modulation equations by averaging three conservation laws (2.7), (2.8) over a 2π period according to

$$\overline{w}_T - \overline{v}_X = 0, \tag{2.11a}$$

$$\overline{v}_T - \overline{f(w)}_X = 0, \tag{2.11b}$$

$$\left(\overline{\phi(w)} + \frac{1}{2}\overline{v^2} + \frac{\omega^2}{24}\overline{w_\theta^2}\right)_T - \left(\overline{vf(w)} - \frac{\omega^2}{12}\overline{w_\theta v_\theta}\right)_X = 0, \tag{2.11c}$$

accompanied by the conservation of waves

$$S_{XT} = S_{TX} \quad \Longleftrightarrow \quad k_T + \omega_X = 0. \tag{2.11d}$$

An additional conservation law, derivable from the previous set, is the average of momentum (2.9)

$$\left(\overline{wv} - \frac{1}{12}k\omega\overline{w_\theta^2}\right)_T - \left(\overline{wf(w)} + \frac{1}{2}\overline{v^2} - \overline{\phi(w)} - \frac{1}{24}\omega^2\overline{w_\theta^2}\right)_X = 0.$$

Here the averaging of a 2π-periodic function $F(\theta)$ is defined according to

$$\overline{F} \equiv \frac{1}{2\pi}\int_0^{2\pi} F(\theta)\,\mathrm{d}\theta.$$

3. Travelling wave solutions

We seek travelling wave solutions of eq. (2.1) in the form

$$u(x,t) = U(\xi), \quad \xi = x - ct, \tag{3.1}$$

where c is the velocity, and ξ is the travelling wave coordinate. Substituting (3.1) into (2.1) and integrating, we obtain

$$c^2\left(w - \frac{1}{12}w''\right) = f(w) - \frac{A}{2}, \tag{3.2}$$

where $w = u_x = U'(\xi)$ is the strain, and A is a constant of integration. Multiplying (3.2) by $w'(\xi)$ and integrating, we obtain

$$(w')^2 = \frac{12}{c^2}(-2\phi(w) + c^2w^2 + Aw + B), \tag{3.3}$$

where B is another integration constant. Equation (2.3) corresponds to

$$\phi(w) = \frac{1}{2}w^2 + \frac{\alpha}{3}w^3 + \frac{\beta}{4}w^4,$$

which together with (3.3) implies that

$$(w')^2 = \frac{12}{c^2}\left(-\frac{\beta}{2}w^4 - \frac{2\alpha}{3}w^3 + (c^2-1)w^2 + Aw + B\right) \tag{3.4}$$

must hold along periodic orbits. If $\beta \neq 0$, we have

$$(w')^2 = -\frac{6\beta}{c^2}G_4(w), \quad G_4(w) = (w-w_1)(w-w_2)(w-w_3)(w-w_4), \tag{3.5}$$

where w_i, $i = 1,\ldots,4$, are the four roots of the quartic polynomial $G_4(w)$, numbered in increasing order of their real parts: $\mathrm{Re}\ w_1 \le \mathrm{Re}\ w_2 \le \mathrm{Re}\ w_3 \le \mathrm{Re}\ w_4$, followed by increasing order in the imaginary

Downloaded from https://www.cambridge.org/core. 16 Nov 2026 at 15:29:29, subject to the Cambridge Core terms of use.

parts. It will be helpful to note the polynomial coefficients of $G_4(w)$:

$$G_4(w) = w^4 + \frac{4\alpha}{3\beta}w^3 - \frac{2}{\beta}(c^2-1)w^2 - \frac{2}{\beta}Aw - \frac{2}{\beta}B. \tag{3.6}$$

In what follows, we will assume that at least two adjacent roots are real, which implies that either all four roots are real, or two are real and the other two are complex conjugates. Phase-plane analysis shows that this assumption is necessary for the existence of real-valued periodic orbits described by (3.5).

We can solve for a constraint on the roots and express c in terms of the roots by equating the coefficients of $G_4(w)$ in (3.5) and (3.6) to obtain

$$-\frac{4\alpha}{3\beta} = w_1 + w_2 + w_3 + w_4, \tag{3.7}$$

$$c^2 = 1 - \frac{\beta}{2}(w_1w_2 + w_1w_3 + w_1w_4 + w_2w_3 + w_2w_4 + w_3w_4). \tag{3.8}$$

Consequently, this is a three-parameter family of travelling wave solutions characterized by, for example, three of the roots. Both signs of c are possible but the root ordering must be maintained, which when w_3 and w_4 are real leads to the constraint

$$w_4 = -\frac{4\alpha}{3\beta} - w_1 - w_2 - w_3 \geq w_3 \quad \Longleftrightarrow \quad w_3 \leq -\frac{2\alpha}{3\beta} - \frac{w_1+w_2}{2}. \tag{3.9}$$

Furthermore, the velocity c in (3.8) must be real, so we also require

$$1 \geq \frac{\beta}{2}(w_1w_2 + w_1w_3 + w_1w_4 + w_2w_3 + w_2w_4 + w_3w_4). \tag{3.10}$$

Equating the two representations (3.5) and (3.6) of $G_4(w)$ also yields expressions for the integration constants in terms of the roots

$$A = \frac{\beta}{2}(w_1w_2w_3 + w_1w_2w_4 + w_1w_3w_4 + w_2w_3w_4), \tag{3.11}$$

$$B = -\frac{\beta}{2}w_1w_2w_3w_4. \tag{3.12}$$

If $\beta = 0$ (α-FPU interaction potential), there are only three roots, all required to be real and numbered in increasing order. In this case, (3.4) reduces to

$$(w')^2 = -\frac{8\alpha}{c^2}G_3(w), \quad G_3(w) = (w-w_1)(w-w_2)(w-w_3), \tag{3.13}$$

The expanded polynomial of $G_3(w)$ from eq. (3.4) is

$$G_3(w) = w^3 - \frac{3}{2\alpha}(c^2-1)w^2 - \frac{3}{2\alpha}Aw - \frac{3}{2\alpha}B. \tag{3.14}$$

Equating the coefficients of $G_3(w)$ in (3.13) and (3.14) determines the velocity-root relation

$$c^2 = 1 + \frac{2\alpha}{3}(w_1 + w_2 + w_3), \tag{3.15}$$

Downloaded from https://www.cambridge.org/core. 16 Nov 2026 at 15:29:29, subject to the Cambridge Core terms of use.

which requires $\frac{2\alpha}{3}(w_1 + w_2 + w_3) > -1$ for real c. Thus, we again obtain a three-parameter family of travelling wave solutions. The coefficient relations of $G_3(w)$ also determine

$$A = -\frac{2\alpha}{3}(w_1w_2 + w_1w_3 + w_2w_3), \tag{3.16}$$

$$B = \frac{2\alpha}{3}w_1w_2w_3. \tag{3.17}$$

Once α and β are fixed, the three-parameter family of travelling waves is parameterized by (c, A, B) or, equivalently, by (w_1, w_2, w_3). Below, we will identify an additional, physical parameterization $(k, a, \overline{w})$ corresponding to the periodic travelling wave's wavenumber k, amplitude a and mean $\overline{w}$.

Although we will obtain three-parameter families of periodic travelling wave solutions for strain w, the regularized Boussinesq equation also requires the determination of particle velocity v in (2.7), which will introduce another integration constant. To fix this, we insert the travelling wave ansatz into the first equation in (2.7) and integrate to obtain

$$v(\xi) = -cw(\xi) + V, \tag{3.18}$$

where V is the integration constant. Averaging the latter expression over the period L of the travelling wave in terms of ξ, we obtain V as a mean accelerated particle velocity

$$V = \overline{v} + c\overline{w} = \frac{1}{L}\int_0^L (v(\xi) + cw(\xi))\,\mathrm{d}\xi.$$

The periodic travelling wave solution (2.10) satisfying (3.4) can be parameterized by the roots w_1, w_2, w_3 and the mean particle velocity $\overline{v}$. Collecting these into the vector

$$\mathbf{W} = (w_1, w_2, w_3, \overline{v})^T, \tag{3.19}$$

we will later consider alternative mathematically and physically convenient parameterizations.

We start by considering the general cubic nonlinearity (2.3) with $\beta \neq 0$ and the orbit described by (3.5). First, we observe that in this case (3.2) becomes

$$w'' = 12\left((c^2 - 1)w - \alpha w^2 - \beta w^3 + \frac{A}{2}\right). \tag{3.20}$$

In what follows, we assume that the right-hand side of this equation has three real roots, corresponding to equilibrium points $(w, w') = (w_*, 0)$ in the phase plane. These equilibria are centres if $c^2 < c_s^2(w_*)$ and saddles if $c^2 > c_s^2(w_*)$. Depending on α and β, the phase plane of (3.20) for given c and A has either two centres separated by a saddle point (Fig. 1(a)) or two saddle points with a centre in between (Fig. 1(b)). Hence, the number of homoclinic orbits that enclose families of periodic trajectories is either two or one, respectively. Below, we consider these two cases separately.

3.1. *Case I:* $\beta > 0$*, two centres*

As illustrated in Fig. 1(a), in this case there are two centres separated by a saddle point and thus two families of periodic orbits described by (3.5), with $w_1 \leq w \leq w_2$ (below the saddle point) and $w_3 \leq w \leq w_4$ (above it), respectively. The first family of orbits is enclosed by the homoclinic trajectory corresponding to a compressive (depression or dark) solitary wave, and the second by a homoclinic orbit corresponding to a tensile (elevation or bright) solitary wave.

Downloaded from https://www.cambridge.org/core. 16 Nov 2026 at 15:29:29, subject to the Cambridge Core terms of use.

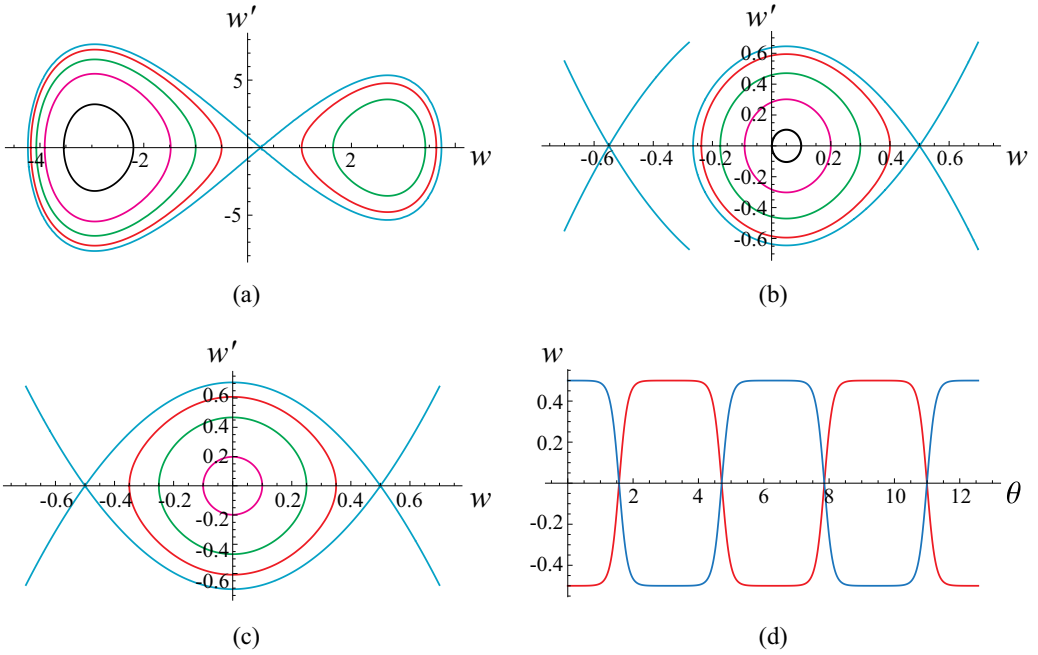


Figure 1. *(a) Periodic orbits for different values of B at $\alpha = 0$, $\beta = 1$, $c = 3$, $A = -127/32$. The orbits on the left of the saddle point correspond to solutions (3.21) with $m = 0.442$, $n = 0.889$, $a = 3.677$ (red), $m = 0.216$, $n = 0.694$, $a = 3.07$ (green), $m = 0$, $n = 0.581$, $a = 2.427$ (magenta), $n = 0.255 - 0.049i$, $a = 1.342$ (black). The orbits on the right correspond to the second family of solutions obtained via (3.33), with the same roots w_i as the orbits of the same colour on the left but amplitude $a = w_4 - w_3$ given by $a = 2.595$ (red) and $a = 1.779$ (green). (b) Periodic orbits at $\alpha = 0$, $\beta = -1$, $c = 0.85$, $A = 11/400$ corresponding to (3.41) with $m = 0.902$, $n = 0.557$, $a = 0.638$ (red), $m = 0.769$, $n = 0.445$, $a = 0.474$ (green), $m = 0.565$, $n = 0.297$, $a = 0.291$ (magenta), $m = 0.239$, $n = 0.111$, $a = 0.099$ (black). (c) Periodic orbits at $\alpha = 0$, $\beta = -1$, $c = \sqrt{3}/2$, $A = 0$ corresponding to (3.41) with $m = 0.924$, $n = 0.726$, $a = 0.7$ (red), $m = 0.796$, $n = 0.549$, $a = 0.5$ (green), $m = 0.4375$, $n = 0.25$, $a = 0.2$ (magenta). (d) Solutions (3.41) (red) and its symmetric counterpart (blue) in the case (c) near the kink limit $m = n = a = 1$. In panels (a–c), manifolds associated with the saddle points (including homoclinic and heteroclinic orbits) are shown in cyan.*

To obtain the first family, we need to solve (3.5) for $w(\xi)$ in the interval (w_1, w_2), where w_1 and w_2 must be real and distinct. Using separation of variables and an appropriate substitution to evaluate the integral involving w [4], we obtain

$$w(\theta) = \frac{w_1 + w_4 n\,\mathrm{sn}^2\left(\frac{K(m)}{\pi}\theta; m\right)}{1 + n\,\mathrm{sn}^2\left(\frac{K(m)}{\pi}\theta; m\right)}, \quad m = \frac{(w_4 - w_3)(w_2 - w_1)}{(w_4 - w_2)(w_3 - w_1)}, \quad n = \frac{w_2 - w_1}{w_4 - w_2}, \tag{3.21}$$

where sn is the Jacobi elliptic sine function and $K(m)$ is the complete elliptic integral of the first kind. The solution (3.21) is 2π-periodic, $w(\theta + 2\pi) = w(\theta)$, in the phase $\theta = k\xi = kx - \omega t$ with wavenumber k and nonlinear frequency ω given by

$$k = \frac{\pi}{K(m)}\sqrt{\frac{3\beta}{2c^2}(w_4 - w_2)(w_3 - w_1)}, \quad \omega = ck, \tag{3.22}$$

Downloaded from https://www.cambridge.org/core. 16 Nov 2026 at 15:29:29, subject to the Cambridge Core terms of use.

where we recall (3.8), the wavelength $L = 2\pi/k$, and the temporal period $T = 2\pi/\omega$. The physical parametrization of this solution is $(k, a, \overline{w})$, where the wavenumber k in (3.22), the amplitude $a = w_2 - w_1$ and the mean

$$\overline{w} = \frac{1}{2\pi}\int_0^{2\pi} w(\theta)\,\mathrm{d}\theta = w_4 - \frac{\Pi(-n,m)}{K(m)}(w_4 - w_1) \tag{3.23}$$

are all determined in terms of the roots w_1, w_2, w_3 in view of (3.7). The function $\Pi(-n, m)$ is the complete elliptic integral of the third kind with n given in (3.21).

Note that the solution (3.21) only requires w_1 and w_2 to be real and also works in the case when w_3 and w_4 are non-real complex conjugates. In this case, m and n are complex but the solution itself and k, a, $\overline{w}$ are real. An example of a periodic orbit with complex $w_{3,4}$ is the black trajectory in Fig. 1(a). In the case when w_3 and w_4 are real, the root ordering $w_1 < w_2 < w_3 < w_4$ implies that

$$n > 0, \quad 0 < m < 1. \tag{3.24}$$

If these roots are complex conjugates, $w_{3,4} = \rho \mp i\eta$, $\eta > 0$, (3.7) implies that $\rho = -(4\alpha/(3\beta)+w_1+w_2)/2$, and the ordering $w_2 < \rho$ thus means that $4\alpha + 3\beta(w_1 + 3w_2) < 0$, which together with $w_1 < w_2$ yields

$$\begin{aligned} \mathrm{Re}(n) &= -\frac{6\beta(w_2 - w_1)(4\alpha + 3\beta(w_1 + 3w_2))}{36\beta^2\eta^2 + (4\alpha + 3\beta(w_1 + 3w_2))^2} > 0, \\ \mathrm{Im}(n) &= -\frac{36\beta^2\eta(w_2 - w_1)}{36\beta^2\eta^2 + (4\alpha + 3\beta(w_1 + 3w_2))^2} < 0. \end{aligned} \tag{3.25}$$

As we will show below, in this case, we can obtain m in terms of real and imaginary parts of n.

The bifurcation from real to complex conjugate roots occurs in the limit $w_3 \to w_4$ where $m \to 0$ so that the solution (3.21) is the trigonometric wave

$$w(\theta) = \frac{w_1 + w_4 n \sin^2(\theta/2)}{1 + n\sin^2(\theta/2)}, \tag{3.26}$$

whose wavenumber, amplitude and mean are

$$k = 2\sqrt{\frac{3\beta}{2c^2}(w_4 - w_2)(w_4 - w_1)}, \quad a = w_2 - w_1, \quad \overline{w} = w_4 - \frac{w_4 - w_1}{\sqrt{1+n}}. \tag{3.27}$$

Since $2w_4 = -4\alpha/(3\beta) - w_1 - w_2$ by virtue of (3.7), the trigonometric wave (3.26) is a two-parameter family of solutions. An example orbit given by the trigonometric solution (3.26) is the magenta trajectory in Fig. 1(a).

In the limit $w_2 \to w_1$ in eq. (3.21), $m \to 0$, and the solution exhibits the following asymptotic behaviour:

$$w(\theta) = w_1 - \frac{1}{2}(w_2 - w_1)\cos\theta + \ldots, \quad \theta = kx - \omega_0 t,$$

where, upon utilizing (3.7), (3.8), (3.22) and (3.23), we obtain the linear dispersion relation (2.4) for small-amplitude (linear) waves propagating on the constant background $\overline{w} = w_1$.

Downloaded from https://www.cambridge.org/core. 16 Nov 2026 at 15:29:29, subject to the Cambridge Core terms of use.

In the limit $w_2 \to w_3$, $m \to 1$, and the solution (3.21) approaches the depression solitary wave

$$w(\xi) = \frac{w_1 + w_4 n \tanh^2(\xi/\ell)}{1 + n\tanh^2(\xi/\ell)}, \quad n = \frac{w_3 - w_1}{w_4 - w_3}, \quad \ell = \left(\frac{3\beta}{2c^2}(w_4 - w_3)(w_3 - w_1)\right)^{-1/2}, \tag{3.28}$$

with amplitude $a = w_3 - w_1$ propagating on the background $\overline{w} = w_3$. An example of the corresponding trajectory is shown by the left cyan loop in Fig. 1(a). These depression solitary waves form a two-parameter family of solutions with velocity-amplitude relation

$$c^2 = c_s^2(\overline{w}) + \frac{1}{2}a^2\beta - \frac{2}{3}a(\alpha + 3\beta\overline{w}). \tag{3.29}$$

Strict inequality $w_3 < w_4$ and (3.7) imply that these waves exist when

$$\overline{w} < -\frac{\alpha}{3\beta}, \; a > 0 \quad \text{or} \quad a > 4\left(\overline{w} + \frac{\alpha}{3\beta}\right) > 0, \tag{3.30}$$

which means that $c^2 > c_s^2(\overline{w})$ in (3.29), and thus the waves are supersonic. Note that this implies that for $\overline{w} > -\alpha/(3\beta)$ the amplitude has a strictly positive *lower bound*.

In the limit $w_2 \to w_3 \to w_4$, we have $\ell \to \infty$, so that $\tanh^2(\xi/\ell) \sim (\xi/\ell)^2$ in eq. (3.28), and the algebraically decaying depression solitary wave is obtained,

$$w(\xi) = \frac{2w_1 - 3\beta w_4\left(w_1(w_4 + w_1) - (w_4 - w_1)^2\xi^2\right)}{2 - 3\beta\left(w_4(w_4 + w_1) - (w_4 - w_1)^2\xi^2\right)}, \tag{3.31}$$

with amplitude $a = w_4 - w_1$ and background $\overline{w} = w_4$. By virtue of (3.7), this is a one-parameter family of algebraic solitary waves subject to the amplitude-background constraint $a = 4(\overline{w} + \alpha/(3\beta)) > 0$. These waves propagate with *sound* velocity,

$$c^2 = 1 + 3\beta\overline{w}(\tfrac{1}{2}a - \overline{w}) = c_s^2(\overline{w}), \tag{3.32}$$

and thus represent the nontrivial sonic limit of (3.28) [37]. The algebraic solitary wave solution (3.31) can alternatively be obtained by taking the limit $w_2 \to w_4$ in the trigonometric wave (3.26) because in this limit $k \to 0$ while $n \to \infty$, so that $n\sin^2(k\xi) \sim n(k\xi)^2 \to 6\beta(w_4 - w_1)^2\xi^2/c^2$.

The second periodic travelling wave family (illustrated by the right set of orbits in Fig. 1(a)) solves (3.5) in (w_3, w_4) with real and distinct w_3 and w_4. It is readily obtained from the first family by using the symmetry of the problem, which amounts to making the following replacements in (3.21):

$$\begin{aligned} &w(\theta) \to -w(\theta) - \frac{2\alpha}{3\beta}, \\ &w_1 \to -w_4 - \frac{2\alpha}{3\beta}, \quad w_2 \to -w_3 - \frac{2\alpha}{3\beta}, \quad w_3 \to -w_2 - \frac{2\alpha}{3\beta}, \end{aligned} \tag{3.33}$$

where the roots are renumbered to keep their nondecreasing order. The solution has the amplitude $a = w_4 - w_3$ and the same wavenumber (3.22), wavelength, frequency and period as the solutions (3.21). It leads to a two-parameter family of trigonometric solutions in the limit $w_2 \to w_1$, a two-parameter elevation solitary wave family in the limit $w_3 \to w_2$, and a one-parameter family of sonic algebraic elevation waves when $w_3 \to w_2 \to w_1$.

For simplicity, we now consider $(\alpha, \beta) = (0, 1)$, recalling that one can always reduce the case $\beta > \alpha^2/3$ to these parameter values upon a proper rescaling, as discussed in Section 2.1. The periodic travelling wave solution (3.21) can be parameterized by $\mathbf{W}$ in (3.19), which involves the first three

Downloaded from https://www.cambridge.org/core. 16 Nov 2026 at 15:29:29, subject to the Cambridge Core terms of use.

roots and the mean particle velocity. First, we consider the case when all four roots are real. In this case, (3.7) and (3.8) for $\alpha = 0$ and $\beta = 1$ imply

$$c^2 = 1 + \frac{1}{4}\left((w_1 + w_2)^2 + (w_2 + w_3)^2 + (w_1 + w_3)^2\right) \geq 1,$$

so that c is always real (eq. (3.10) holds), and we have $|c| \geq 1$. A second, useful parameterization involves the elliptic function parameters n, m, and the wave amplitude a:

$$\mathbf{A} = (n, m, a, \overline{v})^T. \tag{3.34}$$

The transformation $\mathbf{W} = \mathbf{W}(\mathbf{A})$ and its Jacobian determinant are

$$\begin{aligned} &w_1 = a\Xi(n,m)\gamma_1(n,m), \quad w_2 = a\Xi(n,m)\gamma_2(n,m), \quad w_3 = a\Xi(n,m)\gamma_3(n,m), \\ &\Xi = \frac{1}{4n(m+n)}, \quad \det\left(\frac{\partial \mathbf{W}}{\partial \mathbf{A}}\right) = \frac{a^2(1+n)}{4n^2(m+n)^2}, \end{aligned} \tag{3.35}$$

where

$$\begin{aligned} &\gamma_1 = -3n^2 - 2(1+m)n - m, \quad \gamma_2 = n^2 - 2n(1-m) - m, \\ &\gamma_3 = n^2 + 2n(1-m) - m. \end{aligned}$$

For $a > 0$ and (3.24), the transformation (3.35) is invertible. In these variables, the existence of periodic travelling waves is restricted by (3.24):

$$\mathbf{A} \in E_a = \left\{(n, m, a, \overline{v})^T \in \mathbb{R}^4 \,|\, n > 0,\ 0 < m < 1,\ a > 0\right\}. \tag{3.36}$$

Another parameterization results by transforming a in $\mathbf{A}$ to the wave frequency

$$\omega = \operatorname{sgn}(c)\frac{\pi a}{K(m)}\sqrt{\frac{3(1+n)}{2n(m+n)}}, \tag{3.37}$$

which is invertible when (3.36) holds. Similar transformations to k and $\overline{w}$ can also be obtained.

For the case of complex conjugate roots $w_{3,4} = -\frac{1}{2}(w_1 + w_2) \mp i\eta$, $\eta > 0$, it is convenient to use

$$\tilde{\mathbf{A}} = (n_r, n_i, a, \overline{v})^T \tag{3.38}$$

as the parametrisation, where $n_r = \operatorname{Re}(n) > 0$ and $n_i = \operatorname{Im}(n) < 0$ by (3.25). This yields the transformation $\mathbf{W}(\tilde{\mathbf{A}})$

$$\begin{aligned} &w_1 = -\frac{a}{4}\left(3 + \frac{2n_r}{n_i^2 + n_r^2}\right), \quad w_2 = \frac{a}{4}\left(1 - \frac{2n_r}{n_i^2 + n_r^2}\right), \quad w_3 = \frac{a}{4}\left(1 + \frac{2n_r}{n_i^2 + n_r^2}\right) + i\frac{an_i}{n_i^2 + n_r^2}, \\ &\det\left(\frac{\partial \mathbf{W}}{\partial \tilde{\mathbf{A}}}\right) = \frac{ia^2}{2(n_i^2 + n_r^2)^2}, \end{aligned} \tag{3.39}$$

that is invertible for $a > 0$ with

$$m = \frac{2n_i}{n_i + i(1 + n_r)}.$$

Downloaded from https://www.cambridge.org/core. 16 Nov 2026 at 15:29:29, subject to the Cambridge Core terms of use.

Recalling (3.25) and (3.10), we observe that periodic travelling waves exist when

$$\tilde{\mathbf{A}} \in \tilde{E}_a = \Big\{ (n_r, n_i, a, \overline{v})^T \in \mathbb{R}^4 \,|\, n_r > 0,\ n_i < 0,\ a > 0, \\ 16 + a^2 \left(3 + \frac{4(n_i^2(n_r - 2) + n_r^2(1 + n_r))}{(n_i^2 + n_r^2)^2} \right) > 0 \Big\}. \tag{3.40}$$

The transition from real roots to a pair of complex conjugate roots occurs when $w_3 \to w_4$, so that $m \to 0$. Passing to this limit in (3.35), (3.37) and (3.27) for $(\alpha, \beta) = (0, 1)$, we can eliminate n and identify the crossover dispersion relation

$$\omega^2 = k^2 \frac{48 + 9a^2}{48 - 2k^2}, \quad 0 \le k < 2\sqrt{6},$$

holding for the trigonometric solution (3.26) with wave speed satisfying $c^2 = 1 + \frac{3}{16}a^2 + \frac{1}{24}\omega^2$.

3.2. Case II, $\beta < 0$, single centre

In this case, as shown in Fig. 1(b), there are two saddle points separated by a centre, and hence periodic orbits satisfy (3.5) in (w_2, w_3), where w_2 and w_3 are real and distinct. One family of periodic travelling waves is given by [6]

$$w(\theta) = \frac{w_2 - w_1 n \,\mathrm{sn}^2\left(\frac{K(m)}{\pi}\theta; m\right)}{1 - n \,\mathrm{sn}^2\left(\frac{K(m)}{\pi}\theta; m\right)}, \quad m = \frac{(w_4 - w_1)(w_3 - w_2)}{(w_4 - w_2)(w_3 - w_1)}, \quad n = \frac{w_3 - w_2}{w_3 - w_1}, \tag{3.41}$$

where root ordering $w_1 < w_2 < w_3 < w_4$ implies

$$0 < n < m < 1. \tag{3.42}$$

The physical parameters $(k, a, \overline{w})$ are the wavenumber

$$k = \frac{\pi}{K(m)} \sqrt{\frac{3|\beta|}{2c^2}(w_4 - w_2)(w_3 - w_1)}, \tag{3.43}$$

the non-negative amplitude $a = w_3 - w_2$, and the mean strain

$$\overline{w} = w_1 + \frac{\Pi(n, m)}{K(m)}(w_2 - w_1). \tag{3.44}$$

Examples of orbits computed using (3.41) are shown in Figure 1(b).

In the limit $w_3 \to w_2$, $m \to 0$, and

$$w(\theta) = w_2 - \frac{1}{2}(w_3 - w_2)\cos(\theta) + \ldots, \quad \theta = kx - \omega_0 t,$$

subject to the linear dispersion relation (2.4) with $\overline{w} = w_2$.

Downloaded from https://www.cambridge.org/core. 16 Nov 2026 at 15:29:29, subject to the Cambridge Core terms of use.

When $w_3 \to w_4$, $m \to 1$ and we obtain a two-parameter family of depression solitary waves [36]

$$w(\xi) = \frac{w_2 - w_1 n \tanh^2(\xi/\ell)}{1 - n\tanh^2(\xi/\ell)}, \quad n = \frac{w_4 - w_2}{w_4 - w_1}, \quad \ell = \left(\frac{3|\beta|}{2c^2}(w_4 - w_2)(w_4 - w_1)\right)^{-1/2}, \tag{3.45}$$

with amplitude $a = w_4 - w_2$, propagating on the background $\overline{w} = w_4$ with velocity-amplitude relation

$$c^2 = c_s^2(\overline{w}) + \frac{1}{2}\beta a^2 - \frac{2}{3}a(\alpha + 3\beta\overline{w}). \tag{3.46}$$

An example of the corresponding homoclinic trajectory is shown by the cyan loop in Fig. 1(b). Using root ordering $w_1 < w_2 < w_4$, (3.7) and requiring that $c^2 > 0$ in (3.46), we obtain the existence conditions

$$0 < a < 2\left(\overline{w} + \frac{\alpha}{3\beta}\right), \quad \overline{w} + \frac{\alpha}{3\beta} > 0, \quad c_s^2(\overline{w}) + \frac{1}{2}\beta a^2 - \frac{2}{3}a(\alpha + 3\beta\overline{w}) > 0. \tag{3.47}$$

Note that these conditions impose an *upper bound* on the amplitude of the solitary wave, as well as upper and lower bounds on $\overline{w}$, in contrast to the waves (3.28), whose amplitude can be arbitrarily large for any $\overline{w}$ but may have a strictly positive lower bound (recall (3.30)). We also remark that the first two conditions in (3.47) imply that the solitary waves are supersonic, i.e., $c^2 > c_s^2(\overline{w})$ in (3.46), and thus the third inequality is automatically satisfied when $c_s^2(\overline{w}) \geq 0$. However, this inequality must be imposed when $c_s^2(\overline{w}) < 0$ to ensure that $c^2 > 0$.

Another family of periodic travelling waves is related to the first family via the symmetry transformation (3.33). One can show that the two families differ by a π shift in phase θ and have the same mean, wave number and amplitude. In the limit $w_2 \to w_1$, the second family of periodic orbits approaches the two-parameter family of elevation solitary waves that can be obtained from (3.45) using (3.33).

The case in which $w_2 \to w_1$ and $w_3 \to w_4$ results in heteroclinic orbits described by supersonic kink solutions that are given by [36]

$$w(\xi) = \frac{w_1 + w_4}{2} \pm \frac{w_4 - w_1}{2}\tanh(\xi/\ell), \quad \ell = \frac{2|c|}{\sqrt{6|\beta|}(w_4 - w_1)}, \tag{3.48}$$

where

$$w_1 + w_4 = -\frac{2\alpha}{3\beta}, \quad c^2 = 1 - \frac{\alpha^2}{3\beta} + \beta\left(w_1 + \frac{\alpha}{3\beta}\right)^2. \tag{3.49}$$

This is a one-parameter family of kink and antikink solutions. If the plus sign is chosen in (3.48), $w(\xi) \to w_4$ as $\xi \to \infty$ and $w(\xi) \to w_1$ as $\xi \to -\infty$ (an antikink). With the minus sign, we have $w(\xi) \to w_1$ as $\xi \to \infty$ and $w(\xi) \to w_4$ as $\xi \to -\infty$ (a kink). The amplitude $a = w_4 - w_1$ of the kink is the upper bound (3.47) of the solitary wave amplitude for solutions (3.45) and their symmetric counterparts. When $(\alpha, \beta) = (0, -1)$, we have $w_1 = -w_4$, $c^2 = 1 - w_1^2 = 1 - w_4^2$ by (3.49), and the solution (3.48) simplifies to

$$w(\xi) = \pm w_4 \tanh\left(w_4\sqrt{\frac{6}{1 - w_4^2}}\,\xi\right).$$

Examples of periodic orbits approaching the heteroclinic ones are shown in Fig. 1(c). The two families of periodic solutions yield the same trajectories. Near the heteroclinic orbits, the solution acquires the flat-top structure of a periodic kink-antikink lattice shown in Fig. 1(d).

Downloaded from https://www.cambridge.org/core. 16 Nov 2026 at 15:29:29, subject to the Cambridge Core terms of use.

In what follows, we consider the case $(\alpha,\beta) = (0,-1)$ without loss of generality. The periodic travelling wave solution (3.41) can be parameterized by $\mathbf{W}$ in (3.19) subject to the existence inequalities (3.9) and (3.10). As before, we can also introduce the alternative parameterization $\mathbf{A}$ in (3.34) involving the amplitude a.

The transformation $\mathbf{W} = \mathbf{W}(\mathbf{A})$ and its Jacobian determinant are

$$\begin{aligned} &w_1 = a\Xi(n,m)\gamma_1(n,m), \quad w_2 = a\Xi(n,m)\gamma_2(n,m), \quad w_3 = a\Xi(n,m)\gamma_3(n,m), \\ &\Xi = \frac{1}{4n(m-n)}, \quad \det\left(\frac{\partial \mathbf{W}}{\partial \mathbf{A}}\right) = \frac{a^2(1-n)}{4n^2(m-n)^2}, \end{aligned} \tag{3.50}$$

where

$$\begin{aligned} &\gamma_1 = -n^2 + 2(1+m)n - 3m, \quad \gamma_2 = 3n^2 - 2n(1+m) + m, \\ &\gamma_3 = -n^2 - 2n(1-m) + m. \end{aligned}$$

When $a > 0$ and (3.42) hold, the transformation (3.50) is invertible. Periodic travelling wave existence is subject to (3.42) and a real wave speed requiring (3.10):

$$\begin{aligned} \mathbf{A} \in E_a &= \left\{ (n,m,a,\overline{v})^T \in \mathbb{R}^4 \,|\, 0 < n < m < 1,\ 0 < a < a_{\max}(n,m) \right\}, \\ a_{\max} &= \frac{\sqrt{2}}{\Xi(n,m)P(n,m)}, \end{aligned}$$

where

$$\begin{aligned} P(n,m) &= \sqrt{\gamma_1\gamma_2 + \gamma_1\gamma_3 + \gamma_2\gamma_3 - (\gamma_1+\gamma_2+\gamma_3)^2} \\ &= \sqrt{6n^4 - 8(1+m)n^3 + 4(2+m+2m^2)n^2 - 8m(1+m)n + 6m^2}. \end{aligned}$$

The amplitude upper bound $a_{\max}(n,m)$ is an increasing function of its arguments with $a_{\max}(0,0) = a_{\max}(0,m) = \lim_{n\to m} a_{\max}(n,m) = 0$ for $0 < m < 1$ and $\lim_{n\to 1}\lim_{m\to 1} a_{\max}(n,m) = 2$ so that all periodic travelling waves are constrained to have amplitudes in the interval $0 < a < 2$.

We can obtain other parameterizations by, for example, transforming a in $\mathbf{A}$ to the wave frequency

$$\omega = \operatorname{sgn}(c)\frac{\pi a}{K(m)}\sqrt{\frac{3(1-n)}{2n(m-n)}},$$

which is invertible when (3.42) holds. Similar transformations to k and $\overline{w}$ can also be obtained.

3.3. *Case III: $\beta = 0$, single family of periodic orbits*

In this case, eq. (3.20) has a quadratic polynomial in the right-hand side, and we focus on the case of two real roots, corresponding to two equilibrium points $(w_*, 0)$ in the phase plane. If $\alpha > 0$, there is a saddle point on the left, and a centre on the right, so that the homoclinic trajectory enclosing the periodic orbits corresponds to a tensile (bright) solitary wave (see Figure 2). If $\alpha < 0$, the centre is on the left, and the saddle is on the right so that the homoclinic trajectory corresponds to a compressive (dark) solitary

Downloaded from https://www.cambridge.org/core. 16 Nov 2026 at 15:29:29, subject to the Cambridge Core terms of use.

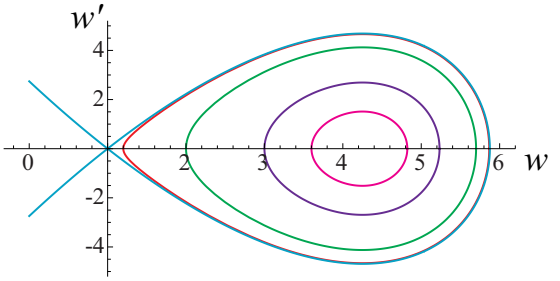


Figure 2. *Periodic orbits for different values of B at $\alpha = 1$, $\beta = 0$, $c = 2.5$, $A = -8.5$ corresponding to (3.51) with $m = 0.9225$, $a = 4.6671$, $\overline{w} = 2.8434$ (red), $m = 0.66971$, $a = 3.6995$, $\overline{w} = 3.5976$ (green), $m = 0.3994$, $a = 2.2333$, $\overline{w} = 4.0457$ (purple), $m = 0.22765$, $a = 1.2224$, $\overline{w} = 4.1915$ (magenta). Manifolds associated with the saddle point (including the homoclinic orbit) are shown in cyan.*

wave. Recall that, in this case, the periodic orbits satisfy (3.13). For $\alpha > 0$, we have $w_2 \le w \le w_3$, and the solution is given by [25]

$$w(\theta) = w_3 - (w_3 - w_2)\mathrm{sn}^2\left(\frac{K(m)}{\pi}\theta\right), \quad m = \frac{w_3 - w_2}{w_3 - w_1}, \tag{3.51}$$

with amplitude $a = w_3 - w_2$, wavenumber

$$k = \frac{\pi}{K(m)}\sqrt{\frac{2|\alpha|}{c^2}(w_3 - w_1)} \tag{3.52}$$

and mean

$$\overline{w} = w_1 + (w_3 - w_1)\frac{E(m)}{K(m)}, \tag{3.53}$$

where $E(m)$ is the complete elliptic integral of the second kind. Example trajectories are shown in Fig. 2.

The harmonic limit when $w_3 \to w_2$, and thus $m \to 0$, is described by

$$w(\theta) = w_2 + \frac{1}{2}(w_3 - w_2)\cos(\theta) + \ldots, \quad \theta = kx - \omega_0 t,$$

with ω_0 corresponding to the linear dispersion relation (2.4) on the background $\overline{w} = w_2$. In the limit $w_2 \to w_1$, $m \to 1$, and we obtain the two-parameter family of elevation solitary waves

$$w(\xi) = w_3 - (w_3 - w_1)\tanh^2(\xi/l), \quad l = \left(\frac{2\alpha}{c^2}(w_3 - w_1)\right)^{-1/2},$$

with amplitude $a = w_3 - w_1$, propagating on the background $\overline{w} = w_1$ with velocity-amplitude relation

$$c^2 = c_s^2(\overline{w}) + \frac{2\alpha}{3}a,$$

where we used (3.15). See the cyan loop in Fig. 2 for an example of the corresponding homoclinic orbit.

Downloaded from https://www.cambridge.org/core. 16 Nov 2026 at 15:29:29, subject to the Cambridge Core terms of use.

For $\alpha < 0$, we have $w_1 \le w \le w_2$, and the solution can be obtained from (3.51) using the symmetry transformation

$$w(\theta) \to -w(\theta), \quad w_3 \to -w_1, \quad w_2 \to -w_2, \quad w_1 \to -w_3,$$

where again the roots are renumbered to keep their nondecreasing order. In the limit when $w_2 \to w_3$, it yields a family of depression solitary waves.

In what follows, we assume $\alpha = 1$. In addition to the parameterization $\mathbf{W}$ in (3.19) in terms of the roots, it is advantageous to introduce the parameterization

$$\overline{\mathbf{A}} = (m, a, \overline{v}, \overline{w})^T. \tag{3.54}$$

The transformation $\mathbf{W} = \mathbf{W}(\overline{\mathbf{A}})$ and its Jacobian determinant are

$$w_1 = \frac{m\overline{w}K(m) - aE(m)}{mK(m)}, \quad w_2 = \frac{mK(m)(\overline{w} - a) - a(E(m) - K(m))}{mK(m)},$$
$$w_3 = \frac{m\overline{w}K(m) - a(E(m) - K(m))}{mK(m)}, \quad \det\left(\frac{\partial \mathbf{W}}{\partial \overline{\mathbf{A}}}\right) = -\frac{a}{m^2},$$

demonstrating invertibility for $a > 0$ and $m > 0$.

The positivity of the squared wave speed (3.15) implies that the mean strain (3.53) exhibits the lower bound

$$\overline{w} > \overline{w}_{\min} = a\frac{3E(m) - (2-m)K(m)}{3mK(m)} - \frac{1}{2}. \tag{3.55}$$

The minimum mean is a decreasing function of m, exhibiting the limits $\lim_{m\to 1} \overline{w}_{\min} = -\frac{1}{2} - \frac{a}{3}$, $\lim_{m\to 0} \overline{w}_{\min} = -\frac{1}{2} + \frac{\omega_0^2}{24}$. Thus, the minimum mean satisfies

$$-\frac{a}{3} \le \overline{w}_{\min} + \frac{1}{2} \le \frac{\omega_0^2}{24}. \tag{3.56}$$

The periodic travelling wave existence criteria are

$$\overline{\mathbf{A}} \in \overline{E}_a = \left\{ (m, a, \overline{v}, \overline{w})^T \in \mathbb{R}^4 \,|\, 0 \le m \le 1,\ a > 0,\ \overline{w} > \overline{w}_{\min} \right\}. \tag{3.57}$$

It first attains the value $\overline{w}_{\min} = -\frac{1}{2}$ when $m = m_* \approx 0.96115$ satisfying $3E(m_*) - (2 - m_*)K(m_*) = 0$. That is, for $0 < m < m_*$, the periodic travelling wave existence criteria include $\overline{w} > \overline{w}_{\min}(m, a) > -\frac{1}{2}$. When $m_* \le m \le 1$, $\overline{w} > \overline{w}_{\min}(m, a) \ge -\frac{1}{2} - \frac{a}{3}$, i.e., the mean can fall below the value $-\frac{1}{2}$. It will be convenient for later analysis to express the admissible set $\overline{E}_a$ as the union of two (not disjoint) subsets

$$\begin{aligned} \overline{E}_a &= \overline{E}_a^{(a)} \cup \overline{E}_a^{(b)}, \\ \overline{E}_a^{(\mathrm{a})} &= \left\{ \overline{\mathbf{A}} \in \mathbb{R}^4 \,|\, 0 < m < 1,\ 0 < a < a_{\max}(m, \overline{w}),\ \overline{w} > -\frac{1}{2} \right\}, \\ \overline{E}_a^{(\mathrm{b})} &= \left\{ \overline{\mathbf{A}} \in \mathbb{R}^4 \,|\, m_* \approx 0.96115 < m < 1,\ 0 < a,\ \overline{w}_{\min}(m, a) < \overline{w} \right\}. \end{aligned} \tag{3.58}$$

Downloaded from https://www.cambridge.org/core. 16 Nov 2026 at 15:29:29, subject to the Cambridge Core terms of use.

Here, the upper bound on the amplitude of the periodic travelling wave is

$$a_{\max}(m,\overline{w}) = \begin{cases} 3\left(\frac{1}{2}+\overline{w}\right)\frac{mK(m)}{3E(m)-(2-m)K(m)}, & 0 < m < m_*, \\ \infty, & m_* < m < 1. \end{cases} \tag{3.59}$$

Since

$$\omega = \operatorname{sgn}(c)\frac{\pi\sqrt{2a/m}}{K(m)}, \tag{3.60}$$

we can invertibly transform $a \to \omega$ in (3.54) within the admissible region.

When $a \to a_{\max}$ for $0 < m < m_*$, the periodic travelling wave velocity $c \to 0$ but the frequency ω remains finite so that the wavenumber $k \to \infty$. Consequently, this is the short-wavelength limit.

4. Whitham modulation equations

The Whitham modulation equations are obtained from an ansatz consisting of a slowly varying periodic travelling wave [39]. The modulation equations describe the projection of the PDE dynamics of (2.1) onto the manifold of periodic travelling waves constrained by a quasilinear system of first-order PDEs of hydrodynamic type [14].

There are several equivalent approaches to obtain the modulation equations. Perhaps the simplest is the average conservation law approach described in Section 2.3. Insertion of the appropriate periodic travelling wave family (one of eqs. (3.21), (3.41), (3.51)) into eq. (2.11) yields the Whitham modulation equations directly. One benefit of this approach is that the conservation form is obtained immediately. One drawback to this form of the modulation equations is that a direct computation of the solitary-wave limit is singular because $k \to 0$ and one of the averaged conservation laws, e.g., (2.11c), is equivalent to (2.11a) and (2.11b) in this limit. Consequently, one equation for the modulations is not determined.

Another mathematically appealing approach to the derivation of the Whitham modulation equations is the method of multiple scales. A suitable ansatz and solvability conditions result in the modulation equations [16].

Yet another approach to obtain the Whitham modulation equations is the averaged variational principle [39]. Integrating the Lagrangian $\mathbb{L}(\theta)$ in eq. (2.6) over a period of the travelling wave family leads to the average Lagrangian $\mathcal{L}(\mathbf{r}) = \frac{1}{2\pi}\int_0^{2\pi}\mathbb{L}(\theta)\,\mathrm{d}\theta$, where $\mathbf{r} \in \mathbb{R}^4$ are the periodic travelling wave's parameters. The Euler-Lagrange equations for the averaged Lagrangian are the Whitham modulation equations. One benefit of this approach is that an additional conservation law, the conservation of wave action

$$\partial_T\mathcal{L}_\omega - \partial_X\mathcal{L}_k = 0,$$

persists in the solitary-wave limit $k \to 0$. In what follows, we use the averaged Lagrangian method to obtain the Whitham modulation equations.

4.1. Averaged conservation laws revisited

Recall that the averaged conservation laws are given by (2.11). Averaging of a 2π-periodic function $F(\theta)$ can now be expressed as

$$\overline{F} = \frac{1}{2\pi}\int_0^{2\pi}F(\theta)\,\mathrm{d}\theta = \frac{|c|k}{2\pi\sqrt{6|\beta|}}\oint\frac{F(w)}{\sqrt{|G_4(w)|}}\,\mathrm{d}w,$$

Downloaded from https://www.cambridge.org/core. 16 Nov 2026 at 15:29:29, subject to the Cambridge Core terms of use.

in the case of the quartic potential $\phi(w)$. For example, taking three roots, say w_1, w_2, w_3 incorporating the constraint (3.7), and the averaged particle velocity $\overline{v}$ in (3.18) as the modulation parameters $\mathbf{W} = (w_1, w_2, w_3, \overline{v})$, eqs. (2.11) are four quasilinear modulation equations for $\mathbf{W}$. The first conservation law (2.11a) is $\overline{w}_T - \overline{v}_X = 0$, where $\overline{w}$ is defined in terms of the roots w_j through (3.8) and one of (3.23) or (3.44) or (3.53), respectively. Using $\omega = ck$, eq. (3.8) and one of (3.22), (3.43), (3.52) for k, the conservation of waves (2.11d) gives another modulation equation. The average velocity (2.11b) and energy (2.11c) equations require further calculation of the density and fluxes. Rather than pursue this further, we instead develop the averaged variational principle.

4.2. Average Lagrangian

Writing the Lagrangian density (2.6) in terms of $u(x,t)$, we obtain

$$\mathbb{L}(u_t, u_x, u_{xt}) = \frac{1}{2}u_t^2 - \phi(u_x) + \frac{1}{24}u_{xt}^2, \quad \phi'(u_x) = f(u_x) \tag{4.1}$$

and note that it depends only on derivatives of $u(x,t)$. Furthermore, the periodic travelling wave solutions are obtained for $v = u_t$ and $w = u_x$. Consequently, the most general periodic travelling wave can be written as

$$u(x,t) = \overline{w}x + \overline{v}t + U(\theta), \quad U(\theta + 2\pi) = U(\theta), \quad \theta = kx - \omega t. \tag{4.2}$$

The term $\overline{w}x + \overline{v}t$ corresponds to the so-called pseudo-phase and enables $U(\theta)$ to be 2π-periodic.

In the general case (2.3), the Lagrangian density (4.1) is

$$\mathbb{L} = \frac{1}{2}u_t^2 - \frac{1}{2}u_x^2 - \frac{1}{3}\alpha u_x^3 - \frac{1}{4}\beta u_x^4 + \frac{1}{24}u_{xt}^2. \tag{4.3}$$

Note that (4.2) implies that $u_t = \overline{v} - c(w(\theta) - \overline{w})$, $u_x = w(\theta)$ and $u_{xt} = -\omega w'(\theta)$, so that (4.3) can be written solely in terms of $w = w(\theta)$

$$\mathbb{L} = \frac{1}{2}\left(\overline{v} - c(w - \overline{w})\right)^2 - \frac{1}{2}w^2 - \frac{\alpha}{3}w^3 - \frac{\beta}{4}w^4 + \frac{1}{24}\omega^2(w')^2.$$

Recalling that, in view of (3.4), we have

$$\frac{\omega^2(w')^2}{24} = -\frac{\beta}{4}w^4 - \frac{\alpha}{3}w^3 + \frac{1}{2}(c^2 - 1)w^2 + \frac{1}{2}Aw + \frac{1}{2}B, \tag{4.4}$$

we arrive at

$$\mathbb{L} = \frac{1}{12}\omega^2(w')^2 - \left(c^2\overline{w} + \overline{v}c + \frac{1}{2}A\right)w + \frac{1}{2}\overline{v}^2 + \frac{1}{2}c^2\overline{w}^2 + c\,\overline{v}\,\overline{w} - \frac{1}{2}B.$$

Thus, the averaged Lagrangian density is given by

$$\mathcal{L}(\overline{w}, \overline{v}, k, \omega, A, B) = \frac{1}{2\pi}\int_0^{2\pi} \mathbb{L}(\theta)\,\mathrm{d}\theta = \frac{\omega^2}{12k}\mathcal{W}\left(\frac{\omega}{k}, A, B\right) + \frac{1}{2}\overline{v}^2 - \frac{\omega^2}{2k^2}\overline{w}^2 - \frac{1}{2}A\overline{w} - \frac{1}{2}B,$$

where

$$\begin{aligned}\mathcal{W}(c, A, B) &= \frac{k}{2\pi}\int_0^{2\pi}(w'(\theta))^2 d\theta = \frac{1}{2\pi}\oint kw'(\theta)dw \\ &= \frac{1}{2\pi}\oint\left[\frac{12}{c^2}\left(-\frac{\beta}{2}w^4 - \frac{2\alpha}{3}w^3 + (c^2 - 1)w^2 + Aw + B\right)\right]^{1/2} dw.\end{aligned} \tag{4.5}$$

Downloaded from https://www.cambridge.org/core. 16 Nov 2026 at 15:29:29, subject to the Cambridge Core terms of use.

Here, we used (4.4), and the integration in w is around the periodic orbit.

The variational equations along with the consistency relations are [39]

$$\begin{aligned} &\mathcal{L}_A = 0, \quad \mathcal{L}_B = 0, \\ &\frac{\partial}{\partial T}\mathcal{L}_\omega - \frac{\partial}{\partial X}\mathcal{L}_k = 0, \quad k_T + \omega_X = 0, \\ &\frac{\partial}{\partial T}\mathcal{L}_{\overline{v}} + \frac{\partial}{\partial X}\mathcal{L}_{\overline{w}} = 0, \quad \overline{w}_T - \overline{v}_X = 0. \end{aligned} \tag{4.6}$$

The first equation, $\mathcal{L}_A = 0$, yields

$$\overline{w} = \frac{c\omega \mathcal{W}_A}{6},$$

which is automatically satisfied because, by (3.5) or (3.13) and (4.5), we have

$$\mathcal{W}_A = \begin{cases} \dfrac{6|c|}{2\pi c^2\sqrt{6|\beta|}} \oint \dfrac{w\, dw}{\sqrt{|G_4(w)|}}, & \beta \neq 0 \\ \dfrac{6|c|}{2\pi c^2\sqrt{8|\alpha|}} \oint \dfrac{w\, dw}{\sqrt{|G_3(w)|}}, & \beta = 0, \end{cases}$$

which in either case yields

$$\mathcal{W}_A = \frac{6}{2\pi c^2 k}\int_0^{2\pi} w d\theta = \frac{6}{c\omega}\overline{w}.$$

The second equation in (4.6), $\mathcal{L}_B = 0$, implies that

$$k = \frac{6}{\mathcal{W}_B c^2},$$

which yields the dispersion relation

$$\omega^2 = (ck)^2 = \frac{6}{k\mathcal{W}_B}.$$

We also have the identity

$$\mathcal{W}_c = -\frac{1}{c}\mathcal{W} + \frac{12\overline{w^2}}{\omega}.$$

The remaining four equations in (4.6) yield

$$\overline{w}_T - \overline{v}_X = 0, \tag{4.7a}$$

$$\overline{v}_T - (c^2\overline{w} + \frac{1}{2}A)_X = 0, \tag{4.7b}$$

$$\left(\frac{c}{12}\mathcal{W} + c\frac{\overline{w^2} - \overline{w}^2}{k}\right)_T + \left(c^2\frac{\overline{w^2} - \overline{w}^2}{k}\right)_X = 0, \tag{4.7c}$$

$$k_T + \omega_X = 0. \tag{4.7d}$$

Downloaded from https://www.cambridge.org/core. 16 Nov 2026 at 15:29:29, subject to the Cambridge Core terms of use.

Here, (4.7a) and (4.7d) coincide with (2.11a) and (2.11d), respectively, while (4.7b) is equivalent to (2.11b) because, by (3.2), we have

$$c^2\overline{w} + \frac{1}{2}A = \overline{f(w) + \frac{\omega^2}{12}w''(\theta)} = \overline{f(w)}.$$

Equation (4.7c) is the conservation of wave action, which makes (4.7) consistent with (2.11) but, as we will see, remains distinct from the remaining equations in the limit $k \to 0$, whereas eq. (2.11c) becomes redundant with the remaining modulation equations.

Two special limits are of interest. In the *solitary-wave limit*, we have $k \to 0$, and hence $\omega \to 0$, so that (4.7d) is trivially satisfied. Thus, in this limit, the modulation system consists of three equations (4.7a), (4.7b) and (4.7c) that will be analysed separately for each case. In the *harmonic limit*, we have $\overline{w^2} \to \overline{w}^2$ and $\mathcal{W} \to 0$, while k is nonzero, making the third equation (4.7c) trivial. Thus, the modulation system (4.7) in this limit reduces to three equations, (4.7a), (4.7b) and (4.7d). These equations are given by

$$\begin{aligned} \overline{w}_T - \overline{v}_X &= 0, \\ \overline{v}_T - c_s^2(\overline{w})\overline{w}_X &= 0, \\ \omega_T + \operatorname{sgn}(\omega)\frac{(c_s^2(\overline{w}) - \omega^2/12)^{3/2}}{c_s^2(\overline{w})}\omega_X - \frac{(\alpha + 3\beta\overline{w})\omega}{c_s^2(\overline{w})}\overline{v}_X &= 0, \end{aligned} \tag{4.8}$$

where we recall that $c_s(\overline{w})$ is the sound speed defined in (2.5). We recognize the first two equations as the dispersionless limit of (2.7), as expected. The third equation is found to be equivalent to the modulation equation for linear waves – conservation of waves (4.7d) with $\omega = \omega_0(k, \overline{w})$, the linear dispersion relation (2.4), which can be inverted to yield

$$k(\omega, \overline{w}) = \frac{|\omega|}{\sqrt{c_s^2(\overline{w}) - \omega^2/12}},$$

where we note that $\omega^2 < 12c_s^2(\overline{w})$ by (2.4). The coefficient of ω_X in this equation equals the group velocity $\operatorname{sgn}(\omega)/k_\omega$, while the coefficient of $\overline{v}_X$ is $k_{\overline{w}}/k_\omega$. In both the solitary wave and harmonic limits, the first two mean equations, (4.7a) and (4.7b), decouple from the third.

We will parameterize the Whitham equations (4.7) using a convenient set of modulation variables, i.e., one of $\mathbf{W}$ in (3.19), $\mathbf{A}$ in (3.34), $\tilde{\mathbf{A}}$ in (3.38), or $\overline{\mathbf{A}}$ in (3.54), depending on the situation. Note that (4.7) have the form $\mathbf{P}_T + \mathbf{Q}_X = 0$, where $\mathbf{P}$ and $\mathbf{Q}$ are the density and flux vectors, respectively. For each parametrization $\mathbf{r}$, we can find $\mathbf{P}(\mathbf{r})$ and $\mathbf{Q}(\mathbf{r})$ and rewrite the Whitham modulation equations (4.7) in the hydrodynamic form

$$\mathbf{r}_T + \mathbb{A}(\mathbf{r})\mathbf{r}_X = \mathbf{0}, \tag{4.9}$$

where $\mathbb{A}(\mathbf{r}) = (\partial\mathbf{P}/\partial\mathbf{r})^{-1}\partial\mathbf{Q}/\partial\mathbf{r}$ is obtained using symbolic algebra in Mathematica.

The modulation system $\mathbf{r}_T + \mathbb{A}(\mathbf{r})\mathbf{r}_X = \mathbf{0}$ has four eigenvalue-eigenvector pairs $\{(\lambda_j, \mathbf{z}_j)\}_{j=1}^4$ satisfying

$$\mathbb{A}(\mathbf{r})\mathbf{z}_j(\mathbf{r}) = \lambda_j(\mathbf{r})\mathbf{z}_j(\mathbf{r}), \quad j = 1, 2, 3, 4.$$

We order the eigenvalues first by their real parts and, for complex conjugate eigenvalues, then by their imaginary parts. We say that the modulation system is *strictly hyperbolic* if $\lambda_j \le \lambda_{j+1} \in \mathbb{R}$ and $\lambda_j = \lambda_{j+1}$ if and only if the j^{th} and $(j+1)^{\text{th}}$ modulation equation are equivalent. Here we use an extended definition of strict hyperbolicity (see, e.g., [30]) in which merged characteristic velocities correspond to a reduction in order of the modulation system. For example, this is precisely the case in the solitary wave and harmonic limits of (4.7), where either the conservation of waves (4.7d) or conservation of wave action

Downloaded from https://www.cambridge.org/core. 16 Nov 2026 at 15:29:29, subject to the Cambridge Core terms of use.

(4.7c) are identically zero in the respective limits. Both limits thus maintain strict hyperbolicity of the modulation system provided that $c_s^2(\overline{w}) = f'(\overline{w}) > 0$. The j^{th} characteristic field is said to be *genuinely nonlinear* if [29]

$$\mu_j(\mathbf{r}) = \nabla_{\mathbf{r}}\lambda_j(\mathbf{r}) \cdot \mathbf{z}_j(\mathbf{r}) \neq 0, \quad j = 1, 2, 3, 4. \tag{4.10}$$

Together, strict hyperbolicity and genuine nonlinearity characterize the *convexity* of the system.

In particular, the system of the first two mean equations in (4.8), which decouples from the remaining equation in the harmonic and solitary-wave limits, has eigenvalues $\lambda_{1,2} = \mp c_s(\overline{w})$ and the corresponding eigenvectors $\mathbf{z}_{1,2} = (1, \pm c_s(\overline{w}))^T$, yielding $\mu_{1,2} = \mp f''(\overline{w})/(2\sqrt{f'(\overline{w})})$. This subsystem is strictly hyperbolic as long as $c_s^2(\overline{w}) = f'(\overline{w}) > 0$ and it is genuinely nonlinear when $f''(\overline{w}) \neq 0$.

Considering now the harmonic-limit system (4.8), we find that the eigenvalues are

$$\lambda_1 = -c_s(\overline{w}), \quad \lambda_2 = \operatorname{sgn}(\omega)\frac{(c_s^2(\overline{w}) - \omega^2/12)^{3/2}}{c_s^2(\overline{w})}, \quad \lambda_3 = c_s(\overline{w}),$$

and the corresponding eigenvectors are

$$\mathbf{z}_1 = \left(1, c_s(\overline{w}), \frac{(\alpha + 3\beta\overline{w})c_s(\overline{w})\omega}{\operatorname{sgn}(\omega)(c_s^2(\overline{w}) - \omega^2/12)^{3/2} + c_s^3(\overline{w})}\right)^T, \quad \mathbf{z}_2 = (0, 0, 1)^T,$$
$$\mathbf{z}_3 = \left(1, -c_s(\overline{w}), -\frac{(\alpha + 3\beta\overline{w})c_s(\overline{w})\omega}{\operatorname{sgn}(\omega)(c_s^2(\overline{w}) - \omega^2/12)^{3/2} - c_s^3(\overline{w})}\right)^T,$$

yielding

$$\mu_1 = -\frac{f''(\overline{w})}{2\sqrt{f'(\overline{w})}}, \quad \mu_2 = -\frac{(f'(\overline{w}) - \omega^2/12)^{1/2}}{4f'(\overline{w})}|\omega|, \quad \mu_3 = \frac{f''(\overline{w})}{2\sqrt{f'(\overline{w})}}.$$

Since the harmonic wave frequency is bounded from above (2.4), the system is strictly hyperbolic when $c_s^2(\overline{w}) = f'(\overline{w}) > 0$ and genuinely nonlinear when $f''(\overline{w}) \neq 0$ and $\omega \neq 0$. In particular, in the case $(\alpha, \beta) = (1, 0)$ considered below, the harmonic limit is convex (strictly hyperbolic and genuinely nonlinear) when $\overline{w} > -1/2$ and $\omega \neq 0$. For cubic nonlinearity with $(\alpha, \beta) = (0, 1)$, the harmonic limit system is always strictly hyperbolic, while in the case $(\alpha, \beta) = (0, -1)$ strict hyperbolicity requires $|\overline{w}| < 1/\sqrt{3}$. In both cases, we must have $\omega \neq 0$ and $\overline{w} \neq 0$ for genuine nonlinearity.

4.3. Quadratic nonlinearity: $(\alpha, \beta) = (1, 0)$

We now consider the special case of $(\alpha, \beta) = (1, 0)$. Note that, if $\beta = 0$, we can set $\alpha = 1$ without loss of generality using the transformation $\alpha u \to u$, as noted in Section 2.1. We wish to express the Whitham eqs. (4.7) in terms of the parameter set $\mathbf{W} = (w_1, w_2, w_3, \overline{v})^T$. For this, we will need to calculate

$$\mathcal{W} = \frac{1}{2\pi}\sqrt{\frac{8}{c^2}}\oint \sqrt{-G_3(w)}\,\mathrm{d}w = \frac{1}{\pi}\sqrt{\frac{8}{c^2}}\int_{w_2}^{w_3} \sqrt{-G_3(w)}\,\mathrm{d}w,$$
$$\overline{w^2} = \frac{1}{2\pi}\int_0^{2\pi} w^2(\theta)\,\mathrm{d}\theta = \frac{1}{2\pi}\sqrt{\frac{\omega^2}{8}}\oint \frac{w^2}{\sqrt{-G_3(w)}}\,\mathrm{d}w = \frac{1}{\pi}\sqrt{\frac{\omega^2}{8}}\int_{w_2}^{w_3} \frac{w^2}{\sqrt{-G_3(w)}}\,\mathrm{d}w.$$

Evaluating the elliptic integrals, we obtain [4]

$$\mathcal{W} = \frac{4\sqrt{2}}{15\pi|c|}\frac{(w_3 - w_2)(w_2 - w_1)^2}{\sqrt{w_3 - w_1}}\frac{2(1 - m + m^2)E(m) - (2 - m)(1 - m)K(m)}{m(1 - m)^2}$$

Downloaded from https://www.cambridge.org/core. 16 Nov 2026 at 15:29:29, subject to the Cambridge Core terms of use.

and

$$\overline{w^2} = \frac{|\omega|}{3\sqrt{2}\pi(m-1)^2\sqrt{w_3-w_1}}\Big\{2(w_2-w_1)\Big((1-2m)w_1+(2-m)w_2\Big)E(m) + (m-1)\left((3m-2)w_1^2-2w_1w_2+w_2^2\right)K(m)\Big\}.$$

Using equations (3.15), (3.16), (3.51), (3.52), (3.53) with $\alpha = 1$, we obtain

$$\begin{aligned} A &= -\frac{2}{3}(w_1w_2+w_1w_3+w_2w_3),\\ c^2 &= 1+\frac{2}{3}(w_1+w_2+w_3), \quad \omega = ck,\\ k &= \frac{\sqrt{2}\pi}{|c|K(m)}\sqrt{w_3-w_1}, \quad m = \frac{w_3-w_2}{w_3-w_1},\\ \overline{w} &= w_1+(w_3-w_1)\frac{E(m)}{K(m)}. \end{aligned} \tag{4.11}$$

Consequently, we have expressed each density and flux of the Whitham equations (4.7) in terms of the parameters $\mathbf{W}$ in (3.19).

4.3.1. Solitary-wave limit

We now pass to the solitary-wave limit $w_2 \to w_1$ in the Whitham equations (4.7). The terms in the wave-action density eq. (4.7c) exhibit the limits

$$\begin{aligned} \lim_{w_2\to w_1}\frac{c}{12}\mathcal{W} &= \frac{\sqrt{2}\mathrm{sgn}(c)}{2\pi}\frac{4}{45}(w_3-w_1)^{5/2},\\ \lim_{w_2\to w_1} c\frac{\overline{w^2}-\overline{w}^2}{k} &= \frac{\sqrt{2}\mathrm{sgn}(c)}{2\pi}\frac{2}{3}c^2(w_3-w_1)^{3/2},\\ \lim_{w_2\to w_1}\overline{w} &= w_1,\\ \lim_{w_2\to w_1}\overline{w^2} &= w_1^2,\\ \lim_{w_2\to w_1} c^2 &= 1+\frac{2}{3}(2w_1+w_3). \end{aligned}$$

Since the solitary wave amplitude is $a = w_3 - w_1$ (cf. Section 3.3), we can express the above quantities in terms of $\overline{\mathbf{A}} = (1, a, \overline{v}, \overline{w})^T$ to obtain

$$\overline{w}_T - \overline{v}_X = 0, \tag{4.12a}$$

$$\overline{v}_T - f(\overline{w})_X = 0, \tag{4.12b}$$

$$\left((1+2\overline{w})a^{3/2}+\tfrac{4}{5}a^{5/2}\right)_T + \left(c\left((1+2\overline{w})a^{3/2}+\tfrac{2}{3}a^{5/2}\right)\right)_X = 0, \tag{4.12c}$$

where

$$c^2 = 1+2\overline{w}+\frac{2}{3}a, \quad f(\overline{w}) = \overline{w}+\overline{w}^2.$$

Downloaded from https://www.cambridge.org/core. 16 Nov 2026 at 15:29:29, subject to the Cambridge Core terms of use.

Note that in eq. (4.12c), we have multiplied through by the inconsequential constant $2\pi/(\sqrt{2}\mathrm{sgn}(c))$ to simplify the expression. We recognize eqs. (4.12a) and (4.12b) as the dispersionless limit of eq. (2.7) and eq. (4.12c) is the equation for the solitary-wave amplitude field $a = a(X, T)$. Expanding eq. (4.12c) and replacing $\overline{w}_T = \overline{v}_X$, we obtain

$$a_T + c\, a_X + \frac{4a}{3(1 + 2\overline{w} + \frac{4}{3}a)}\overline{v}_X + \frac{2ca}{1 + 2\overline{w} + \frac{4}{3}a}\overline{w}_X = 0. \tag{4.13}$$

Because it is decoupled from the other equations (4.12a), (4.12b), the characteristic velocity for (4.13) is $\lambda = c$, as it should be in the solitary-wave limit.

Equation (4.12) exhibits the ordered characteristic velocities (for the branch of fast waves with $c > 0$)

$$\lambda_1 = -\sqrt{1 + 2\overline{w}}, \quad \lambda_2 = \sqrt{1 + 2\overline{w}}, \quad \lambda_3 = c = \sqrt{1 + 2\overline{w} + \tfrac{2}{3}a}.$$

The corresponding eigenvectors are

$$\mathbf{z}_1 = \begin{bmatrix} 1 \\ \sqrt{1 + 2\overline{w}} \\ -\dfrac{1+2\overline{w}+2a+\sqrt{(1+2\overline{w})\,(1+2\overline{w}+\frac{2}{3}a)}}{1+2\overline{w}+\frac{4}{3}a} \end{bmatrix}, \quad \mathbf{z}_2 = \begin{bmatrix} 1 \\ \sqrt{1 + 2\overline{w}} \\ -\dfrac{1+2\overline{w}+2a-\sqrt{(1+2\overline{w})\,(1+2\overline{w}+\frac{2}{3}a)}}{1+2\overline{w}+\frac{4}{3}a} \end{bmatrix}, \quad \mathbf{z}_3 = \begin{bmatrix} 0 \\ 0 \\ 1 \end{bmatrix}.$$

4.3.2. Convexity

We first examine the convexity (hyperbolicity, genuine nonlinearity) of the Whitham equations in the solitary-wave limit (4.12). The mean lower bound $\overline{w} > -\frac{1}{2} - \frac{a}{3}$ for solitary waves (recall (3.56)) ensures that $\lambda_3 \in \mathbb{R}$ but it does not preclude the possibility of complex characteristic velocities λ_1 and λ_2. Thus, to ensure strict hyperbolicity, we further require $\overline{w} > -\frac{1}{2}$ and $a > 0$. To assess genuine nonlinearity, we compute

$$\mu_j = \nabla\lambda_j \cdot \mathbf{z}_j = \partial_{\overline{w}}\lambda_j = \frac{1}{\lambda_j} \neq 0, \quad j = 1, 2,$$
$$\mu_3 = \nabla\lambda_3 \cdot \mathbf{z}_3 = \partial_a\lambda_3(a, \overline{w}) = \frac{1}{3\lambda_3} \neq 0.$$

Thus, the solitary-wave modulation system is genuinely nonlinear, provided it is strictly hyperbolic.

We now examine the convexity of the full Whitham system (4.7) by numerically computing the eigenvalues and eigenvectors of the modulation matrix $\mathbb{A}(\mathbf{r})$ in (4.9) as $\overline{\mathbf{A}}$ is varied. Recalling the admissibility criteria (3.57), (3.58), we will study convexity in two separate regimes:

(a) $\overline{E}_a^{(\mathrm{a})}$: $\overline{w} > -\frac{1}{2}$, $0 < a < a_{\max}$, and $0 < m < 1$,
(b) $\overline{E}_a^{(\mathrm{b})}$: $\overline{w}_{\min}(m, a) < \overline{w}$, $a > 0$, and $m_* < m < 1$,

where $\overline{w}_{\min}$ is given by (3.55), $a_{\max}$ is defined in (3.59) and $m_* \approx 0.96115$ satisfies $3\,E(m_*) - (2 - m_*)K(m_*) = 0$. For case (a), we introduce the change of variables

$$\text{(a)} \quad u \to (1 + 2\overline{w})u + \overline{v}t + \overline{w}x, \quad t \to \frac{t}{\sqrt{1 + 2\overline{w}}}, \quad \overline{w} > -\frac{1}{2},$$

to eq. (2.1), leaving it unchanged since $\overline{w} > -\frac{1}{2}$. Consequently, in this case, we will set $\overline{v} = \overline{w} = 0$ without loss of generality and consider variation of the remaining two modulation parameters $0 < m < 1$,

Downloaded from https://www.cambridge.org/core. 16 Nov 2026 at 15:29:29, subject to the Cambridge Core terms of use.

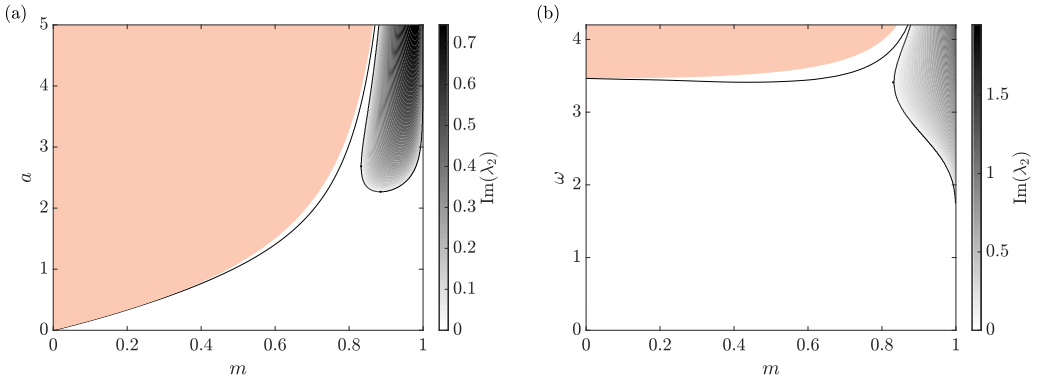


Figure 3. *Hyperbolicity of the regularized Boussinesq–Whitham equations for* $(\alpha, \beta) = (1, 0)$ *(case III), quadratic interaction force with* $\overline{\mathbf{A}} = (m, a, \overline{v} = 0, \overline{w} = 0) \in \overline{E}_a^{(a)}$*: Strict hyperbolicity (white region). Greyscale is the magnitude of the imaginary part of* λ_2 *where the system is not hyperbolic. Periodic travelling waves do not exist in the inadmissible pink region. Black dots depict points corresponding to the values* $(m, a) \in \{(0.83, 2.69),\ (0.89, 2.27)\}$ *in (a) and* $(m, \omega) = (0.83, 3.41)$ *in (b) where complex characteristic velocities are first encountered. The solid black curves correspond to parameters where the second characteristic field loses genuine nonlinearity,* $\mu_2 = \nabla\lambda_2 \cdot \mathbf{z}_2 = 0$*, and* $\lambda_1 = \lambda_2$ *at the boundary of the non-hyperbolic region. Panels (a) and (b) are equivalent under the transformation (3.60).*

$0 < a < a_{\max}(m, \overline{w} = 0)$. For case (b), we note that eq. (2.1) is invariant under the alternative change of variables

$$\text{(b)} \quad u \to \frac{u}{a} + \overline{v}t + \left(\frac{1}{2a} - \frac{1}{2}\right)x, \quad t \to \sqrt{a}t, \quad a > 0,$$

Now, we will set $a = 1$ without loss of generality and consider convexity when $m_* < m < 1$ and $\overline{w} > \overline{w}_{\min}(m, a = 1)$.

Figure 3 depicts the (white) region of strict hyperbolicity when $\overline{\mathbf{A}} \in \overline{E}_a^{(a)}$. We find that $\lambda_3 < \lambda_4$ are real and distinct for all computed admissible parameter values. There exists a greyscale region in which the modulations exhibit complex conjugate characteristic velocities λ_1 and λ_2. Such regions correspond to modulational instability of the underlying periodic travelling wave [39]. At the boundaries of these regions, $\lambda_1 = \lambda_2 \in \mathbb{R}$. The coalescence of two characteristics coincides with loss of genuine nonlinearity, so $\mu_1 = \mu_2 = 0$ also. The smallest values of m and a where complex characteristics occur are depicted as black dots.

We also compute the quantities μ_j in (4.10) in the strictly hyperbolic region and find that only $\mu_2 = 0$ (i.e., $\mu_1 \neq 0$, so $\lambda_1 \neq \lambda_2$) on a curve bifurcating from $(a, m) = (0, 0)$ or $(\omega, m) = (\sqrt{12}, 0)$. The curve is depicted in Fig. 3. Nonzero μ_j is a necessary monotonicity condition for the existence of a j-integral curve in which $\mathbf{r}'(\alpha) = \mathbf{z}_j(\mathbf{r}(\alpha))$ where α evolves along the characteristic $\frac{\mathrm{d}x}{\mathrm{d}t} = \lambda_j$: $\alpha_t + \lambda_j(\mathbf{r}(\alpha))\alpha_x = 0$. Simple waves are used in the solution of the Riemann problem consisting of step initial conditions at the origin. The short-wave limit ($k \to \infty$) occurs when a approaches the pink admissibility boundary ($a \to a_{\max}$). At this boundary, the modulation matrix $\mathbb{A}$ exhibits a double zero eigenvalue and two real, oppositely signed eigenvalues.

Figure 4 depicts hyperbolicity for case (b) where we normalize the amplitude to $a = 1$ and require $\overline{w} > \overline{w}_{\min}$, $m_* \leq m < 1$. We observe that the system is hyperbolic when $\overline{w}$ is sufficiently large. The depicted results are consistent with the solitary-wave limit (4.12) that is strictly hyperbolic for $\overline{w} > -\frac{1}{2}$. The upper dashed curve in Figure 4 where $\lambda_1 = \lambda_2$ limits to $\overline{w} = -\frac{1}{2}$ as $m \to 1$ but the approach is very sharp due to the logarithmic approach of $\overline{w}$ to $-\frac{1}{2}$ because $K(m) \sim -1/\log(1 - m)$ in the mean equation (4.11) as $m \to 1$. In a similar manner, the lower dashed curve in Fig. 4 at the boundary of the

Downloaded from https://www.cambridge.org/core. 16 Nov 2026 at 15:29:29, subject to the Cambridge Core terms of use.

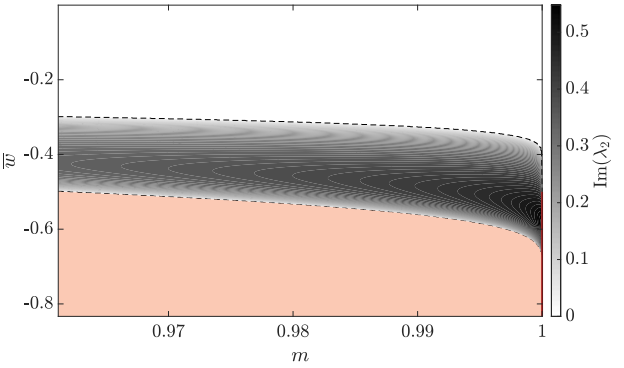


Figure 4. *Hyperbolicity of the regularized Boussinesq–Whitham equations for case III, quadratic interaction force with* $\overline{\mathbf{A}} = (m, a = 1, \overline{v} = 0, \overline{w}) \in \overline{E}_a^{(b)}$*: Strict hyperbolicity (white region). Greyscale is the magnitude of the imaginary part of* λ_2 *where the system is not hyperbolic. At* $m = m_* \approx 0.96115$*, we find that for* $\overline{w} > -0.298$*, the system is strictly hyperbolic. The dashed curves correspond to the boundary of the non-hyperbolic region where* $\lambda_1 = \lambda_2$*, so that* $\mu_1 = \mu_2 = 0$ *there also. Periodic travelling waves do not exist in the inadmissible pink region. The red segment at* $m = 1$ *corresponds to the region of non-hyperbolicity of the solitary-wave limiting system (4.12).*

admissible region also sharply limits to $\overline{w} = \overline{w}_{\min}(a = 1, m = 1) = -\frac{5}{6}$ as $m \to 1$. This demonstrates that the region in Fig. 4 where hyperbolicity is lost bifurcates from the segment $-\frac{5}{6} < \overline{w} < -\frac{1}{2}$ for $m = 1$, which is denoted by the red segment.

4.4. *Cubic nonlinearity with* $(\alpha, \beta) = (0, 1)$

We now consider the case of cubic $f(w)$ with $(\alpha, \beta) = (0, 1)$, to which, as we discussed in Section 2.1, case I in Section 3.1 can be reduced upon a proper rescaling. As before, we need to compute $\mathcal{W}$ and $\overline{w^2}$ that are given by

$$\mathcal{W} = \frac{1}{2\pi}\sqrt{\frac{6}{c^2}}\oint \sqrt{-G_4(w)}\,\mathrm{d}w, \quad \overline{w^2} = \frac{1}{2\pi}\sqrt{\frac{\omega^2}{6}}\oint \frac{w^2}{\sqrt{-G_4(w)}}\,\mathrm{d}w.$$

Recall that in this case we have two families of periodic solutions related by the symmetry transformation (3.33) with $\alpha = 0$ and $\beta = 1$. Thus, it suffices to consider the first solution family (3.21). We have

$$\begin{aligned}
&w_1 + w_2 + w_3 + w_4 = 0,\\
&A = \frac{1}{2}(w_1w_2w_3 + w_1w_2w_4 + w_1w_3w_4 + w_2w_3w_4),\\
&c^2 = 1 - \frac{1}{2}(w_1w_2 + w_1w_3 + w_1w_4 + w_2w_3 + w_2w_4 + w_3w_4),\\
&k = \frac{\pi}{K(m)}\sqrt{\frac{3}{2c^2}(w_4 - w_2)(w_3 - w_1)}, \quad \omega = ck,\\
&m = \frac{(w_4 - w_3)(w_2 - w_1)}{(w_4 - w_2)(w_3 - w_1)},
\end{aligned} \tag{4.14}$$

where we used (3.7), (3.8), (3.11), (3.21) and (3.22).

Downloaded from https://www.cambridge.org/core. 16 Nov 2026 at 15:29:29, subject to the Cambridge Core terms of use.

To find $\mathcal{W}$ and $\overline{w^2}$ we use

$$\mathcal{W} = \frac{1}{\pi}\sqrt{\frac{6}{c^2}}\int_{w_1}^{w_2}\sqrt{(w-w_1)(w_2-w)(w_3-w)(w_4-w)}\,\mathrm{d}w,$$
$$\overline{w^2} = \frac{1}{\pi}\sqrt{\frac{\omega^2}{6}}\int_{w_1}^{w_2}\frac{w^2\,\mathrm{d}w}{\sqrt{(w-w_1)(w_2-w)(w_3-w)(w_4-w)}}.$$

Evaluation of the elliptic integrals yields [4]

$$\begin{aligned}\mathcal{W} = {}& \frac{(w_2-w_1)^2(w_3-w_1)^{1/2}(w_4-w_1)^2}{4|c|\sqrt{6}\pi n^3(1+n)^2(n+m)^2(w_4-w_2)^{3/2}}\Big\{n\Big(3n^4+3m^2+4n^3(1+m)\\ &+4nm(1+m)+2n^2(2+m+2m^2)\Big)E(m)\\ &-(n+m)\Big(3n^4-4n^2(m-1)-3m^2-6nm^2+2n^3(2+m)\Big)K(m)\\ &+3(n^2-m)(2n+n^2+m)(n^2+m+2nm)\Pi(-n,m)\Big\}\end{aligned}$$

and

$$\begin{aligned}\overline{w^2} = {}& \frac{\sqrt{2}w_4^2|\omega|}{\sqrt{3}\pi\sqrt{(w_3-w_1)(w_4-w_2)}}\Big\{K(m)+2\left(\frac{w_1}{w_4}-1\right)\Pi(-n,m)\\ &+\frac{(w_4-w_1)^2}{2(1+n)(n+m)w_4^2}\Big(nE(m)-(n+m)K(m)\\ &+\Big(n^2+3m+2n(1+m)\Big)\Pi(-n,m)\Big)\Big\},\end{aligned}\tag{4.15}$$

where we recall that m and n are given in (3.21) and satisfy (3.24) and (3.25) in the case of real and complex $w_{3,4}$, respectively.

4.4.1. Solitary-wave limit

Recall that in the solitary-wave limit $w_2 \to w_3$ ($m \to 1$), the solutions approach the two-parameter family (3.28) with amplitude $a = w_3 - w_1$, background $\overline{w} = w_3$ and velocity (3.29). In this limit, we obtain

$$\begin{aligned}\lim_{w_2\to w_3}\frac{c}{12}\mathcal{W} &= \frac{\mathrm{sgn}(c)}{\pi\sqrt{6}}\Big\{\frac{1}{6}\sqrt{a(a-4\overline{w})}(a^2-4a\overline{w}+6\overline{w}^2)\\ &\quad+(a-2\overline{w})^2\overline{w}\arctan\sqrt{\frac{a}{a-4\overline{w}}}\Big\},\\ \lim_{w_2\to w_3}c\frac{\overline{w^2}-\overline{w}^2}{k} &= \frac{c^2\mathrm{sgn}(c)}{\pi\sqrt{6}}\Big\{\sqrt{a(a-4\overline{w})}+4\overline{w}\arctan\sqrt{\frac{a}{a-4\overline{w}}}\Big\},\\ \lim_{w_2\to w_3}\overline{w^2} &= \overline{w}^2,\qquad \lim_{w_2\to w_3}c^2 = 1+3\overline{w}^2+\frac{1}{2}a(a-4\overline{w}),\end{aligned}$$

Downloaded from https://www.cambridge.org/core. 16 Nov 2026 at 15:29:29, subject to the Cambridge Core terms of use.

where we recall that either $\overline{w} < 0$ and $a > 0$ or $a > 4\overline{w} > 0$ by (3.30) with $\alpha = 0$. In this limit, the Whitham modulation equations (4.7) with $f(w) = w + w^3$ become

$$\begin{aligned} \overline{w}_T - \overline{v}_X &= 0, \\ \overline{v}_T - (1 + 3\overline{w}^2)\overline{w}_X &= 0, \\ a_T + c\, a_X + c\, \frac{g(a,\overline{w})}{d(a,\overline{w})}\overline{w}_X + \frac{h(a,\overline{w})}{d(a,\overline{w})}\overline{v}_X &= 0, \end{aligned} \tag{4.16}$$

where

$$\begin{aligned} g(a,\overline{w}) &= -\sqrt{a(a-4\overline{w})}(2 + 4a^2 - 19a\overline{w} + 24\overline{w}^2) \\ &\quad + 2(2 + (a-6\overline{w})(a-4\overline{w}))(a-2\overline{w}) \arctan\sqrt{\frac{a}{a-4\overline{w}}}, \\ h(a,\overline{w}) &= -\sqrt{a(a-4\overline{w})}(2 + 4a^2 - 19a\overline{w} + 24\overline{w}^2) \\ &\quad + (4 + 3(a-4\overline{w})^2)(a-2\overline{w}) \arctan\sqrt{\frac{a}{a-4\overline{w}}}, \\ d(a,\overline{w}) &= \sqrt{a(a-4\overline{w})}(1 + 2a^2 - 8a\overline{w} + 9\overline{w}^2) + 6(a-2\overline{w})^2\overline{w} \arctan\sqrt{\frac{a}{a-4\overline{w}}}. \end{aligned} \tag{4.17}$$

The ordered characteristic velocities (for the fast waves with $c > 0$) are

$$\lambda_1 = -\sqrt{1 + 3\overline{w}^2}, \quad \lambda_2 = \sqrt{1 + 3\overline{w}^2}, \quad \lambda_3 = c = \sqrt{1 + 3\overline{w}^2 + \frac{1}{2}a(a - 4\overline{w})}. \tag{4.18}$$

The associated eigenvectors are

$$\mathbf{z}_j = \begin{bmatrix} 1 \\ -\lambda_j \\ \frac{\lambda_j h(a,\overline{w}) - \lambda_3 g(a,\overline{w})}{d(a,\overline{w})(\lambda_3 - \lambda_j)} \end{bmatrix}, \quad j = 1, 2, \quad \mathbf{z}_3 = \begin{bmatrix} 0 \\ 0 \\ 1 \end{bmatrix}. \tag{4.19}$$

In the limit $w_2 \to w_3 \to w_4$ the solitary waves reduce to the one-parameter family (3.31) with background $\overline{w} = w_4$, amplitude $a = w_4 - w_1 = 4\overline{w}$, where the second equality follows from the first equation in (4.14), and velocity (3.32), yielding

$$\begin{gathered} \lim_{w_2 \to w_3 \to w_4} \frac{c}{12}\mathcal{W} = \frac{\operatorname{sgn}(c)}{32\sqrt{6}}a^3, \qquad \lim_{w_2 \to w_3 \to w_4} c\frac{\overline{w^2} - \overline{w}^2}{k} = \frac{c^2 \operatorname{sgn}(c)}{2\sqrt{6}}a, \\ \lim_{w_2 \to w_3 \to w_4} \overline{w^2} = \overline{w}^2, \qquad \lim_{w_2 \to w_3 \to w_4} c^2 = 1 + \frac{3}{16}a^2 = c_s^2(\overline{w}). \end{gathered}$$

In this case, the third equation in (4.16) decouples from the first two and becomes $a_T + c\, a_X = 0$, which for $c > 0$ is equivalent to the fast characteristic family in the first two equations of (4.16), i.e., $\lambda_2 = \lambda_3$. Thus, the algebraic solitary wave (3.31) with $c = c_s(\overline{w}) > 0$ ($c = -c_s(\overline{w}) < 0$) moves with the fast (slow) characteristic velocity of mean evolution.

4.4.2. Convexity

Here, we examine the convexity of the Whitham modulation equations using various means. First, we consider convexity of the solitary-wave modulation system (4.16) analytically and then proceed to assess the convexity of the full modulation equations (4.7) by numerically evaluating the eigenstructure of the modulation matrix $\mathbb{A}$ in (4.9).

The solitary-wave existence conditions $\overline{w} < 0$ and $a > 0$ or $a > 4\overline{w} > 0$ in eq. (3.30) with $\alpha = 0$ for the first solitary-wave family (3.28) imply real characteristic velocities (4.18). When $a = 4\overline{w}$, either

Downloaded from https://www.cambridge.org/core. 16 Nov 2026 at 15:29:29, subject to the Cambridge Core terms of use.

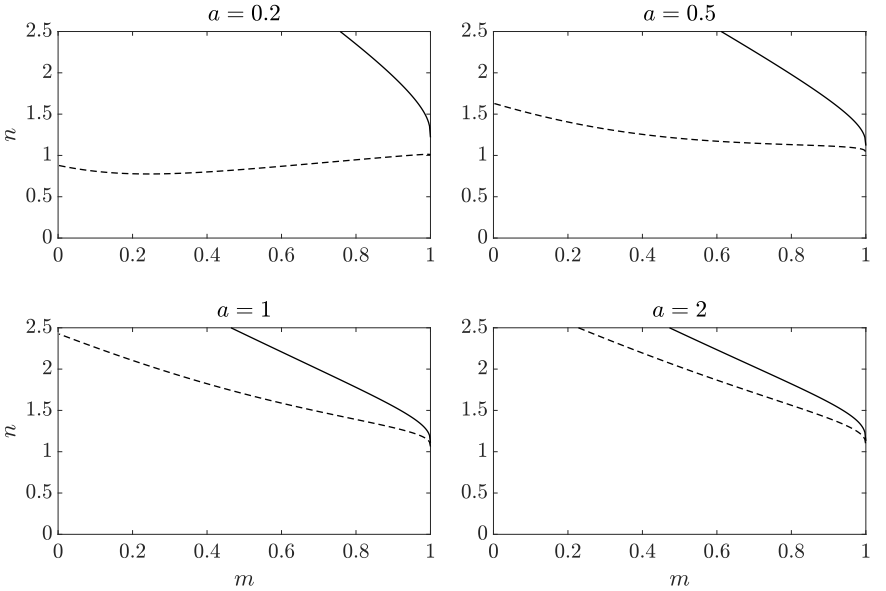


Figure 5. *Convexity of the Whitham modulation equations for* $(\alpha, \beta) = (0, 1)$ *(case I) with real roots* w_j*. For each fixed amplitude a, the solid (dashed) curves correspond to the loss of genuine nonlinearity* $\mu_1 = 0$ *(*$\mu_2 = 0$*) bifurcating from the point* $(n, m) = (1, 1)$ *where the solitary-wave limiting system loses genuine nonlinearity at* $\overline{w} = 0$*.*

$\lambda_2 = \lambda_3$ (for $c > 0$) or $\lambda_1 = c = \lambda_2 = -\sqrt{1 + 3\overline{w}^2}$ (for $c < 0$). This case corresponds to the algebraic solitary wave, whose modulation is equivalent to the fast or slow mean modulation. Consequently, the solitary-wave modulation system (4.16) with (4.17) is strictly hyperbolic.

From (4.18) and (4.19) it follows that the genuine nonlinearity conditions (4.10) are

$$\mu_j = \nabla\lambda_j \cdot \mathbf{z}_j = \partial_{\overline{w}}\lambda_j = \frac{3\overline{w}}{\lambda_j} \neq 0, \quad j = 1, 2,$$

$$\mu_3 = \nabla\lambda_3 \cdot \mathbf{z}_3 = \partial_a\lambda_3(a, \overline{w}) = \frac{a - 2\overline{w}}{2\lambda_3} \neq 0.$$

Consequently, the solitary-wave modulation system (4.16) with (4.17) loses genuine nonlinearity in both of the mean modulation characteristic families at an inflection point of the interaction force $f''(\overline{w}) = 3\overline{w} = 0$. Since either $\overline{w} < 0$ and $a > 0$ or $a > 4\overline{w} > 0$ for solitary wave existence, we have $\mu_3 > 0$.

Thus, the modulation system in the solitary-wave limit is strictly hyperbolic for all parameter values and loses genuine nonlinearity when $\overline{w} = 0$. Recall that the same is true for the harmonic limit in this case. Since $\overline{w} = w_3$, $a = w_3 - w_1$ and $w_4 = -2w_3 - w_1$, the loss of genuine nonlinearity occurs precisely when $n = (w_3 - w_1)/(w_4 - w_3) = 1$.

For the full Whitham modulation system in the case of real roots w_j, we find that the equations are strictly hyperbolic for $n > 0$, $0 < m < 1$. Figure 5 depicts curves in the m-n plane with fixed a where the modulation system loses genuine nonlinearity in one of the first two characteristic families. These curves bifurcate from the $m = 1$ solitary-wave limit at $n = 1$, the inflection point of the interaction force $\overline{w} = 0$ where the solitary wave limiting system (4.16) loses genuine nonlinearity. Since the modulated periodic travelling wave amplitude is held constant, the limit $m \to 0$ corresponds to the trigonometric wave limit where $w_3 \to w_4$.

Downloaded from https://www.cambridge.org/core. 16 Nov 2026 at 15:29:29, subject to the Cambridge Core terms of use.

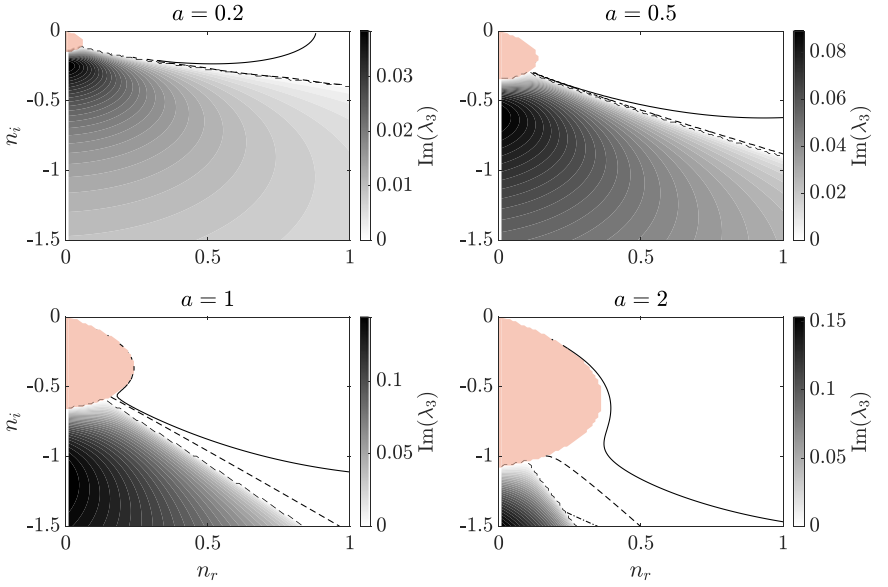


Figure 6. *Convexity of the Whitham modulation equations for* $(\alpha, \beta) = (0, 1)$ *(case I), cubic interaction force with complex conjugate roots* $w_{3,4}$, $\tilde{\mathbf{A}} = (n_r, n_i, a, \overline{v} = 0) \in \tilde{E}_a$*: The system is strictly hyperbolic in the white region. Greyscale is* $\mathrm{Im}(\lambda_3)$ *where the system is not hyperbolic. Periodic travelling waves do not exist in the inadmissible pink region. For each fixed amplitude a, the solid (dashed) curves correspond to the loss of genuine nonlinearity* $\mu_2 = 0$ *(*$\mu_3 = 0$*). For* $a = 2$*, the dash-dotted curve corresponds to* $\mu_1 = 0$*.*

On the other hand, modulations of periodic travelling waves with complex conjugate roots $w_{3,4}$ exhibit strict hyperbolicity in a limited range of the n_r-n_i plane. This is shown in Figure 6 for differing, fixed amplitudes a. Accompanying the loss of hyperbolicity for some parameter regions is the loss of genuine nonlinearity in the first, second and third characteristic fields. The second characteristic field is linearly degenerate along a curve $\mu_2 = 0$ that bifurcates from the trigonometric limit $n_i = 0$. For example, when $a = 0.2$ in Figure 5, the level curve $\mu_2 = 0$ meets the trigonometric limit when $(n, m) \approx (0.878, 0)$. Similarly, in Figure 6 with $a = 0.2$, the curve $\mu_2 = 0$ enters the domain from $(n_r, n_i) \approx (0.878, 0)$. As a varies, the level curves exhibit somewhat complex deformations. The level curve $\mu_1 = 0$ appears within the parameter window of consideration when $a = 2$. The boundary of the non-hyperbolic region is where $\lambda_2 = \lambda_3$, so $\mu_2 = \mu_3 = 0$ there.

4.5. Cubic nonlinearity with $(\alpha, \beta) = (0, -1)$

Next, we discuss the case of cubic $f(w)$ with $(\alpha, \beta) = (0, -1)$, which corresponds to case II in Section 3.2 after an appropriate rescaling discussed in Section 2.1. In this setting, we have

$$\mathcal{W} = \frac{1}{2\pi}\sqrt{\frac{6}{c^2}}\oint \sqrt{G_4(w)}\,\mathrm{d}w = \frac{1}{\pi}\sqrt{\frac{6}{c^2}}\int_{w_2}^{w_3} \sqrt{(w-w_1)(w-w_2)(w_3-w)(w_4-w)}\,\mathrm{d}w,$$

$$\overline{w^2} = \frac{1}{2\pi}\sqrt{\frac{\omega^2}{6}}\oint \frac{w^2}{\sqrt{G_4(w)}}\,\mathrm{d}w = \frac{1}{\pi}\sqrt{\frac{\omega^2}{6}}\int_{w_2}^{w_3} \frac{w^2\,\mathrm{d}w}{\sqrt{(w-w_1)(w-w_2)(w_3-w)(w_4-w)}}.$$

Recall that in this case, there are two families of periodic solutions related by symmetry (3.33) with $\alpha = 0, \beta = -1$ and that differ by a π phase shift, so it suffices to consider one of them given by (3.41).

Downloaded from https://www.cambridge.org/core. 16 Nov 2026 at 15:29:29, subject to the Cambridge Core terms of use.

We have

$$\begin{aligned}
&w_1 + w_2 + w_3 + w_4 = 0,\\
&A = -\frac{1}{2}(w_1w_2w_3 + w_1w_2w_4 + w_1w_3w_4 + w_2w_3w_4),\\
&c^2 = 1 + \frac{1}{2}(w_1w_2 + w_1w_3 + w_1w_4 + w_2w_3 + w_2w_4 + w_3w_4),\\
&k = \frac{\pi}{K(m)}\sqrt{\frac{3}{2c^2}(w_4 - w_2)(w_3 - w_1)}, \quad \omega = ck,\\
&m = \frac{(w_4 - w_1)(w_3 - w_2)}{(w_4 - w_2)(w_3 - w_1)},
\end{aligned}$$

where we used (3.7), (3.8), (3.11), (3.41) and (3.43), and obtain [4]

$$\begin{aligned}
\mathcal{W} = \frac{(w_3 - w_2)^2(w_4 - w_2)^{1/2}(w_2 - w_1)^2}{4|c|\sqrt{6}\pi n^3(1-n)^2(m-n)^2(w_3 - w_1)^{3/2}}\Big\{&n\Big(3n^4 + 3m^2 - 4n^3(1+m)\\
&- 4nm(1+m) + 2n^2(2 + m + 2m^2)\Big)E(m)\\
&+ (m-n)\Big(3n^4 - 4n^2(m-1) - 3m^2 + 6nm^2 - 2n^3(2+m)\Big)K(m)\\
&+ 3(m - n^2)(-2n + n^2 + m)(n^2 + m - 2nm)\Pi(n,m)\Big\}
\end{aligned} \tag{4.20}$$

and

$$\begin{aligned}
\overline{w^2} = \frac{\sqrt{2}w_1^2|\omega|}{\sqrt{3}\pi\sqrt{(w_3 - w_1)(w_4 - w_2)}}\Big\{&K(m) + 2\left(\frac{w_2}{w_1} - 1\right)\Pi(n,m)\\
&+ \frac{(w_2 - w_1)^2}{2(n-1)(m-n)w_1^2}\Big(nE(m) + (m-n)K(m)\\
&- \Big(n^2 + 3m - 2n(1+m)\Big)\Pi(n,m)\Big)\Big\},
\end{aligned} \tag{4.21}$$

where we recall that m and n are given in (3.41) and satisfy (3.42).

4.5.1. Solitary-wave limit

In the limit $w_3 \to w_4$ ($m \to 1$), the solutions approach the two-parameter family (3.45) of solitary waves with amplitude $a = w_4 - w_2$, background $\overline{w} = w_4$ and velocity (3.46). In this limit, we obtain

$$\begin{aligned}
\lim_{w_3\to w_4}\frac{c}{12}\mathcal{W} &= \frac{\mathrm{sgn}(c)}{\pi\sqrt{6}}\Big\{\frac{1}{6}\sqrt{a(4\overline{w} - a)}(a^2 - 4a\overline{w} + 6\overline{w}^2)\\
&\qquad - (a - 2\overline{w})^2\overline{w}\,\mathrm{arctanh}\sqrt{\frac{a}{4\overline{w} - a}}\Big\},\\
\lim_{w_3\to w_4} c\frac{\overline{w^2} - \overline{w}^2}{k} &= \frac{c^2\mathrm{sgn}(c)}{\pi\sqrt{6}}\Big\{-\sqrt{a(4\overline{w} - a)} + 4\overline{w}\,\mathrm{arctanh}\sqrt{\frac{a}{4\overline{w} - a}}\Big\},\\
\lim_{w_3\to w_4}\overline{w^2} &= \overline{w}^2, \quad \lim_{w_3\to w_4} c^2 = 1 - 3\overline{w}^2 + \frac{1}{2}a(4\overline{w} - a),
\end{aligned} \tag{4.22}$$

Downloaded from https://www.cambridge.org/core. 16 Nov 2026 at 15:29:29, subject to the Cambridge Core terms of use.

where we recall that $0 < a < 2\overline{w}$ by (3.47) with $\alpha = 0$. The Whitham modulation equations (4.7) with $f(w) = w - w^3$ therefore become

$$\begin{aligned} \overline{w}_T - \overline{v}_X &= 0, \\ \overline{v}_T - (1 - 3\overline{w}^2)\overline{w}_X &= 0, \\ a_T + c\,a_X + c\,\frac{g(a,\overline{w})}{d(a,\overline{w})}\overline{w}_X + \frac{h(a,\overline{w})}{d(a,\overline{w})}\overline{v}_X &= 0, \end{aligned} \tag{4.23}$$

where

$$\begin{aligned} g(a,\overline{w}) &= \sqrt{a(4\overline{w}-a)}(-2 + 4a^2 - 19a\overline{w} + 24\overline{w}^2) \\ &\quad + 2\Big(-2 + (a-6\overline{w})(a-4\overline{w})\Big)(a-2\overline{w})\,\operatorname{arctanh}\sqrt{\frac{a}{4\overline{w}-a}}, \\ h(a,\overline{w}) &= \sqrt{a(4\overline{w}-a)}(-2 + 4a^2 - 19a\overline{w} + 24\overline{w}^2) \\ &\quad + \Big(-4 + 3(a-4\overline{w})^2\Big)(a-2\overline{w})\,\operatorname{arctanh}\sqrt{\frac{a}{4\overline{w}-a}}, \\ d(a,\overline{w}) &= \sqrt{a(4\overline{w}-a)}(-1 + 2a^2 - 8a\overline{w} + 9\overline{w}^2) - 6(a-2\overline{w})^2\overline{w}\,\operatorname{arctanh}\sqrt{\frac{a}{4\overline{w}-a}}. \end{aligned} \tag{4.24}$$

The ordered characteristic velocities (for the fast-wave family with $c > 0$) are

$$\lambda_1 = -\sqrt{1-3\overline{w}^2}, \quad \lambda_2 = \sqrt{1-3\overline{w}^2}, \quad \lambda_3 = c = \sqrt{1-3\overline{w}^2 + \frac{1}{2}a(4\overline{w}-a)}. \tag{4.25}$$

Note that the existence conditions (3.47) for $(\alpha,\beta) = (0,-1)$ amount to satisfying one of the following inequality pairs

$$\text{either} \quad 0 < a < 2\overline{w} \quad \text{and} \quad 0 < \overline{w} \le \frac{1}{\sqrt{3}}, \tag{4.26a}$$

$$\text{or} \quad 2\overline{w} - \sqrt{2(1-\overline{w}^2)} < a < 2\overline{w} \quad \text{and} \quad \frac{1}{\sqrt{3}} < \overline{w} < 1. \tag{4.26b}$$

The associated eigenvectors are given by (4.19).

4.5.2. Kink limit

The limit $a \to 2\overline{w}$ corresponds to the supersonic kink solution (3.48). To obtain its modulation, it is tempting to send $a \to 2\overline{w}$ in eq. (4.23). But this results in a singularity. Instead, we return to the wave-action equation (4.7c) with the solitary-wave limiting density and flux in eq. (4.22). We denote the limit as $a \to 2\hat{w}$ in order to distinguish the kink $\hat{w}$ from the mean $\overline{w}$. An expansion of the density and flux results in

$$\begin{aligned} \frac{c}{12}\mathcal{W} + c\frac{\overline{w^2} - \overline{w}^2}{k} &= -\frac{2\operatorname{sgn}(c)}{\pi\sqrt{6}}f(\hat{w})\log(2\hat{w}-a) + \mathcal{O}(1), \\ c^2\frac{\overline{w^2} - \overline{w}^2}{k} &= -\frac{2|c|}{\pi\sqrt{6}}f(\hat{w})\log(2\hat{w}-a) + \mathcal{O}(1), \end{aligned}$$

as $a \to 2\hat{w}$ where $f(\hat{w}) = \hat{w} - \hat{w}^3$ is the interaction force and $c^2 = 1 - \hat{w}^2$ is the squared kink velocity (3.49). Inserting this into the conservation of wave action (4.7c), we obtain the expansion

$$\frac{f(\hat{w})}{2\hat{w}-a}\left[(2\hat{w}-a)_T + c(2\hat{w}-a)_X\right] + \log(2\hat{w}-a)\left[f(\hat{w})_T + (cf(\hat{w}))_X\right] + \cdots = 0.$$

Downloaded from https://www.cambridge.org/core. 16 Nov 2026 at 15:29:29, subject to the Cambridge Core terms of use.

Multiplying this expression by $2\hat{w} - a$ and equating each order to zero as $a \to 2\hat{w}$, we obtain the kink conservation law

$$f(\hat{w})_T + [cf(\hat{w})]_X = 0, \quad f(\hat{w}) = \hat{w} - \hat{w}^3, \quad c = \pm\sqrt{1 - \hat{w}^2}.$$

This equation is distinct from the mean equations for $(\overline{w}, \overline{v})$ in (4.23) and admits the discontinuous travelling wave solution

$$\hat{w}(X, T) = \pm 2w_0 \operatorname{sgn}(X - cT), \quad c^2 = 1 - w_0^2, \quad 0 < w_0 < 1, \tag{4.27}$$

whose velocity $s = c$ results from the Rankine–Hugoniot jump condition $-s[f(\hat{w})] + [cf(\hat{w})] = 0$ where $[\cdot]$ is the difference between the state $\cdot$ to the right and left of the discontinuity. The weak solution (4.27) is the zero-dispersion limit of the kink solution (3.48) and thus is an admissible shock. Since the mean field propagates along characteristics with velocities $\lambda_j = \mp\sqrt{f'(\overline{w})} = \mp\sqrt{1 - 3\overline{w}^2}$, they are unchanged on either side of the shock ($f'(w_0) = f'(-w_0)$), i.e., the characteristics pass through the shock. It is because of this that the solution (4.27) can be interpreted as a non-classical, undercompressive shock [17, 23] and is an example of a superkink in the classification of steady transition fronts in mechanical systems [22].

4.5.3. Convexity

We start by considering the modulation system (4.23) with (4.24) for the solitary-wave family (3.45), with eigenvalues (4.25) and eigenvectors (4.19). The existence condition for this family is (4.26). In this case, we obtain

$$\mu_j = -\frac{3\overline{w}}{\lambda_j}, \quad j = 1, 2, \quad \mu_3 = \frac{2\overline{w} - a}{2\lambda_3}.$$

Thus, the system is strictly hyperbolic when $0 < \overline{w} < 1/\sqrt{3}$ and genuinely nonlinear when $a \neq 2\overline{w}$, which ensures that $\mu_3 \neq 0$. Since a nonzero mean is required for the existence of a solitary wave, $\mu_j \neq 0$ for $j = 1, 2$. We recall that the harmonic limit is strictly hyperbolic when $|\overline{w}| < 1/\sqrt{3}$ and genuinely nonlinear when $\overline{w} \neq 0$ and $\omega \neq 0$.

To investigate the convexity of the full Whitham modulation system (4.7) with (4.20) and (4.21), we will present our results in terms of $\mathbf{A}$ in (3.34). For several choices of the periodic travelling wave amplitude a, we plot the existence region and imaginary part of the second eigenvalue in Figure 7. Within the existence region, two islands nucleate where hyperbolicity is lost. The islands take up a larger percentage of the existence region as the wave amplitude is increased. To further understand these islands, we note that the depression solitary-wave limit with $m \to 1$ admits the following relation between the solitary-wave parameters $(a, \overline{w})$ and the parameter n in (3.45)

$$n = \frac{a}{4\overline{w} - a}, \quad 0 < a < 2\overline{w}, \quad \overline{w} > 0, \tag{4.28}$$

by $a = w_4 - w_2$, $\overline{w} = w_4$ and $w_1 + w_2 + 2w_4 = 0$. According to (4.25), we expect the nucleation of non-hyperbolic regions in the second characteristic family from $\overline{w} \geq 1/\sqrt{3}$ in the solitary-wave limit. Indeed, the red segment in Fig. 7 along $m = 1$ corresponds to the values of n in (4.28) satisfying the inequalities (4.26b) that yield $1/\sqrt{3} < \overline{w} < a/3 + \sqrt{2(6 - a^2)}/6$.

Figure 7 also depicts the level curves $\mu_j = 0$. The solid black curve corresponds to both $\mu_1 = 0$ and $\mu_4 = 0$. It bifurcates from the kink limit $m \to 1, n \to 1$. The dashed curves correspond to regions where $\mu_2 = 0$. Necessarily, these surround the non-hyperbolic greyscale regions where $\lambda_1 = \lambda_2$ because the coalescence of two characteristics (non-strict hyperbolicity) coincides with loss of genuine nonlinearity, so that $\mu_1 = 0$ also there.

Downloaded from https://www.cambridge.org/core. 16 Nov 2026 at 15:29:29, subject to the Cambridge Core terms of use.

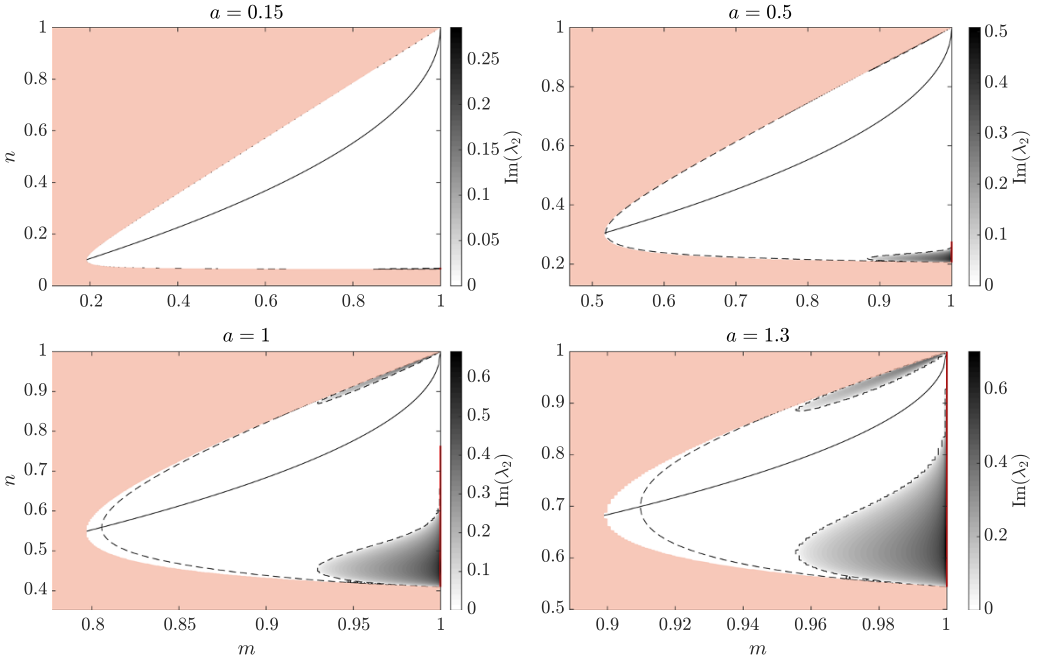


Figure 7. *Hyperbolicity of the Whitham modulation equations for* $(\alpha, \beta) = (0, -1)$ *(case II). For each fixed amplitude a, the greyscale contour plot conveys the imaginary part of a characteristic velocity. Periodic waves do not exist in the inadmissible pink region. The solid (dashed) black curves correspond to the loss of genuine nonlinearity* $\mu_1 = \mu_4 = 0$ *(*$\mu_2 = 0$*). The red segment at* $m = 1$ *corresponds to the region of non-hyperbolicity of the solitary-wave limiting system (4.23).*

5. Stability of periodic travelling waves

The loss of hyperbolicity in the modulation equations discussed in Sections 4.3.2, 4.4.2 and 4.5.3 corresponds to modulational instability of the corresponding periodic travelling wave [39]. To verify the onset of such an instability, we numerically compute the spectrum of the linearized operator for various parameter values and solve initial value problems with suitably perturbed periodic travelling wave initial data.

To obtain the corresponding eigenvalue problem, we first observe that (2.7) is equivalent to

$$w_t = v_x, \qquad v_t = \left(1 - \frac{1}{12}\partial_x^2\right)^{-1} (f(w))_x, \tag{5.1}$$

where we used $w_{tt} = v_{xt}$. Rewriting (5.1) in terms of $w = \tilde{w}(\xi, t)$, $v = \tilde{v}(\xi, t)$, $\xi = x - ct$, we obtain

$$\tilde{w}_t = \tilde{v}_\xi + c\tilde{w}_\xi, \qquad \tilde{v}_t = \left(1 - \frac{1}{12}\partial_\xi^2\right)^{-1} (f(w))_\xi + c\tilde{v}_\xi.$$

Seeking solutions of this system in the form

$$\begin{bmatrix} \tilde{w} \\ \tilde{v} \end{bmatrix} = \begin{bmatrix} W(\xi) \\ V(\xi) \end{bmatrix} + \varepsilon e^{\lambda t} \boldsymbol{\phi}(\xi),$$

Downloaded from https://www.cambridge.org/core. 16 Nov 2026 at 15:29:29, subject to the Cambridge Core terms of use.

where $W(\xi)$ and $V(\xi)$ are the strain and particle velocity for a periodic travelling wave with period T_0,

$$W(\xi + T_0) = W(\xi), \quad V(\xi + T_0) = V(\xi),$$

and keeping only terms of order ε, we obtain the following eigenvalue problem for the linearized operator:

$$\lambda \boldsymbol{\phi} = \begin{bmatrix} c\partial_\xi & \partial_\xi \\ \left(1 - \frac{1}{12}\partial_\xi^2\right)^{-1} \partial_\xi f'(W(\xi)) & c\partial_\xi \end{bmatrix} \boldsymbol{\phi}. \tag{5.2}$$

By Floquet theory applied to the T_0-periodic linear operator in the right-hand side of (5.2), the eigenvalue λ is in the spectrum if and only if there exists a nonzero eigenfunction $\boldsymbol{\phi}$ such that [5]

$$\boldsymbol{\phi}(\xi + T_0) = e^{\frac{2\pi i q \xi}{T_0}} \boldsymbol{\phi}(\xi)$$

for some real q. This implies [2] that there exists $\boldsymbol{\psi}$ such that

$$\boldsymbol{\phi}(\xi + T_0) = e^{\frac{2\pi i \tau \xi}{T_0}} \boldsymbol{\psi}(\xi), \quad \boldsymbol{\psi}(\xi + T_0) = \boldsymbol{\psi}(\xi), \tag{5.3}$$

where $\tau \in (-1/2, 1/2]$ is the Floquet parameter. Thus, we have

$$\boldsymbol{\psi}(\xi) = \sum_{q \in \mathbb{Z}} \hat{\boldsymbol{\psi}}_q \exp \frac{2\pi i q \xi}{T_0} \tag{5.4}$$

where $\hat{\boldsymbol{\psi}}_q$ are the Fourier coefficients of $\boldsymbol{\psi}$. Using (5.2) and (5.3), we obtain

$$\begin{aligned} \lambda \boldsymbol{\psi} &= \begin{bmatrix} c\left(\frac{2\pi i \tau}{T_0} + \partial_\xi\right) & \frac{2\pi i \tau}{T_0} + \partial_\xi \\ M(\tau) f'(W(\xi)) & c\left(\frac{2\pi i \tau}{T_0} + \partial_\xi\right) \end{bmatrix} \boldsymbol{\psi}, \\ M(\tau) &= \left(1 - \frac{1}{12}\left(\frac{2\pi i \tau}{T_0} + \partial_\xi\right)^2\right)^{-1} \left(\frac{2\pi i \tau}{T_0} + \partial_\xi\right). \end{aligned} \tag{5.5}$$

To numerically compute the spectrum of the linear operator, we use the Floquet–Fourier–Hill method [10]. Following the procedure in [2], we restrict the values of q in (5.4) to $q = -N_q, \ldots, N_q$ and use Fourier collocation to project (5.5) to a subspace of $L^2(-T_0/2, T_0/2) \times L^2(-T_0/2, T_0/2)$. This reduces the problem to finding eigenvalues of a $(4N_q + 1) \times (4N_q + 1)$ matrix $\mathbf{L}(\tau)$, which is computed by taking sums and products of diagonal and Toeplitz matrices that represent differential operators and multiplications by periodic functions in (5.5), respectively. Computing these eigenvalues for each value of τ in the N_τ-point discretization of $(-1/2, 1/2]$, we obtain the numerical approximation of the spectrum. In what follows, we use $N_q = 100$ and $N_\tau = 200$. Since $f'(W(\xi)) = 1 + 2\alpha W(\xi) + 3\beta W^2(\xi)$, the procedure requires computing the Fourier coefficients of $W(\xi)$ in the quadratic nonlinearity case $(\alpha, \beta) = (1, 0)$ and $W^2(\xi)$ in the case of cubic nonlinearity, where $(\alpha, \beta) = (0, \pm 1)$. In the case of

Downloaded from https://www.cambridge.org/core. 16 Nov 2026 at 15:29:29, subject to the Cambridge Core terms of use.

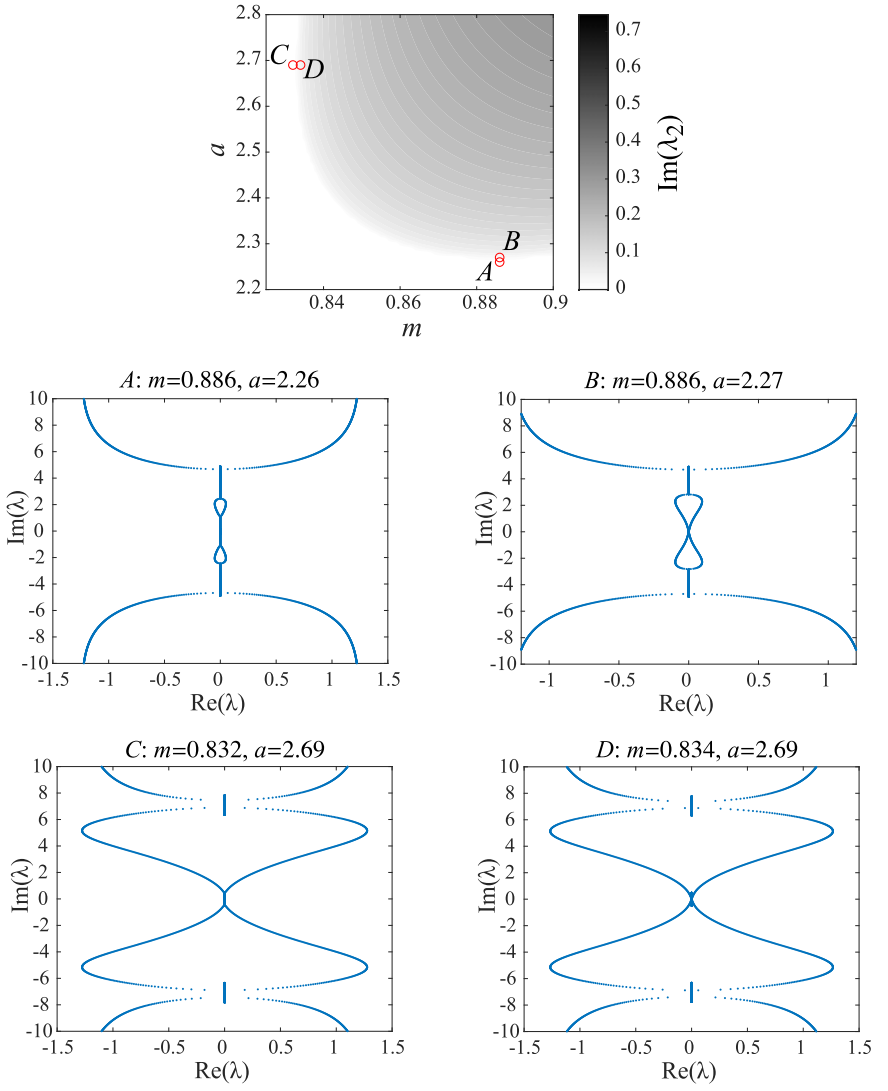


Figure 8. *Top panel: Fig. 3(a) zoomed in around the tip of the grey region where the Whitham system loses hyperbolicity in the case of quadratic nonlinearity ($\alpha = 1$, $\beta = 0$). Middle and bottom panels: spectra of the linear operator at the parameter values marked by points A, B, C and D in the top panel.*

quadratic nonlinearity, the coefficients can be found analytically using the Fourier expansion for $\mathrm{sn}^2(x)$ [28]:

$$W(\xi) = \sum_{q\in\mathbb{Z}} \hat{W}_q e^{\frac{2\pi i q \xi}{T_0}}, \quad \hat{W}_q = \begin{cases} (w_3 - w_2)\frac{\pi^2 q \kappa^q}{mK^2(m)(1-\kappa^{2q})}, & q \neq 0 \\ w_3 - (w_3 - w_2)\frac{K(m)-E(m)}{mK(m)}, & q = 0 \end{cases}, \quad \kappa = \exp\frac{\pi K(1-m)}{K(m)}.$$

For the cubic nonlinearity cases, the Fourier coefficients were computed using numerical integration in Mathematica. To speed up the computations, we took advantage of the fact that these coefficients quickly decay as $|q|$ tends to infinity so we restricted the computed coefficients to $|q| \leq q_{\mathrm{cut}}$, setting the rest to zero. In most cases, $q_{\mathrm{cut}} = 40$ was sufficient.

We begin by examining the spectra in the case of quadratic nonlinearity (Case III) with $(\alpha, \beta) = (1, 0)$. The top panel in Fig. 8 zooms in around the top of the grey region in Fig. 3(a), where the

Downloaded from https://www.cambridge.org/core. 16 Nov 2026 at 15:29:29, subject to the Cambridge Core terms of use.

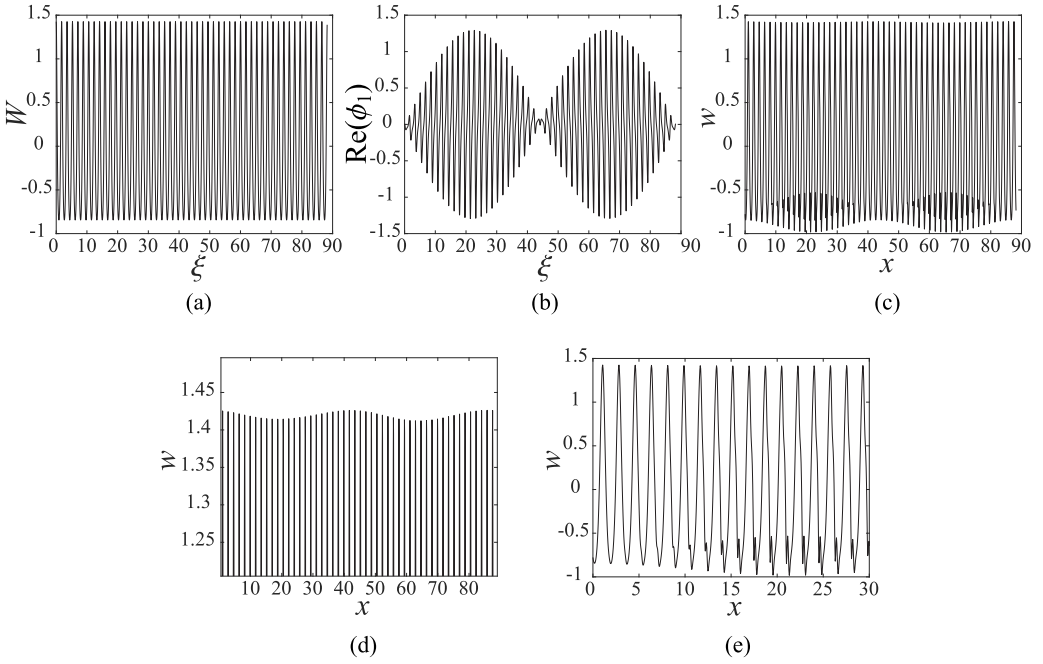


Figure 9. *(a) The strain component $W(\xi)$ of the periodic travelling wave solution at $m = 0.886$, $a = 2.27$. (b) Real part of the first component ϕ_1 of the eigenfunction associated with the eigenvalue $\lambda = 0.0019 + 0.0883i$. (c) Strain profile at $t = 8$ in the dynamical simulation initiated by the travelling wave perturbed by the unstable mode, with perturbation amplitude $\varepsilon = 0.01$. (d) Panel (c) zoomed in around the top part. (e) Panel (c) zoomed in around the left part.*

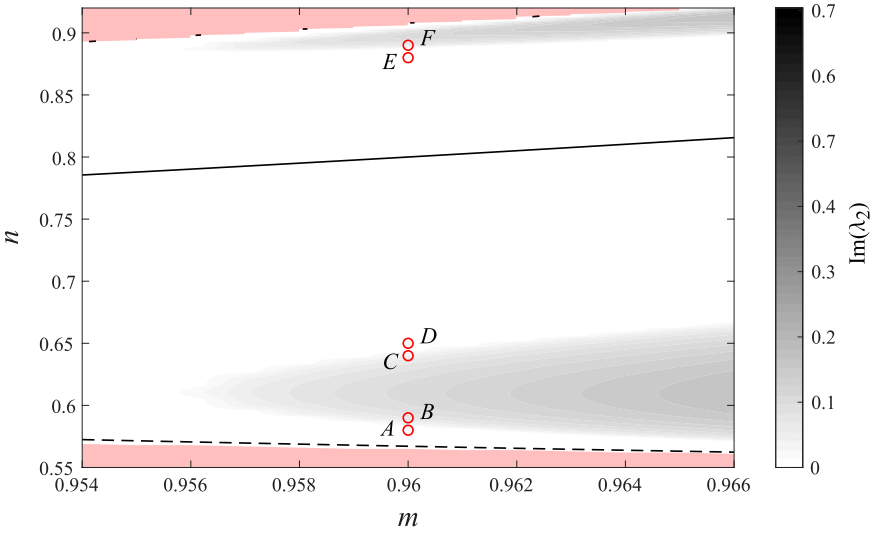


Figure 10. *Fig. 7(d) ($a = 1.3$) zoomed in near the tips of the grey regions where the Whitham system loses hyperbolicity in the case of cubic nonlinearity with $(\alpha, \beta) = (0, -1)$. Spectra shown in Fig. 11 were computed at the parameter values marked by the points A-F.*

Whitham modulation system loses hyperbolicity. As we enter this region, we expect to see the onset of modulational instability of periodic travelling waves. To check this, we compute the linear spectrum for periodic travelling waves at the parameter values m and a corresponding to points A and B, located

Downloaded from https://www.cambridge.org/core. 16 Nov 2026 at 15:29:29, subject to the Cambridge Core terms of use.

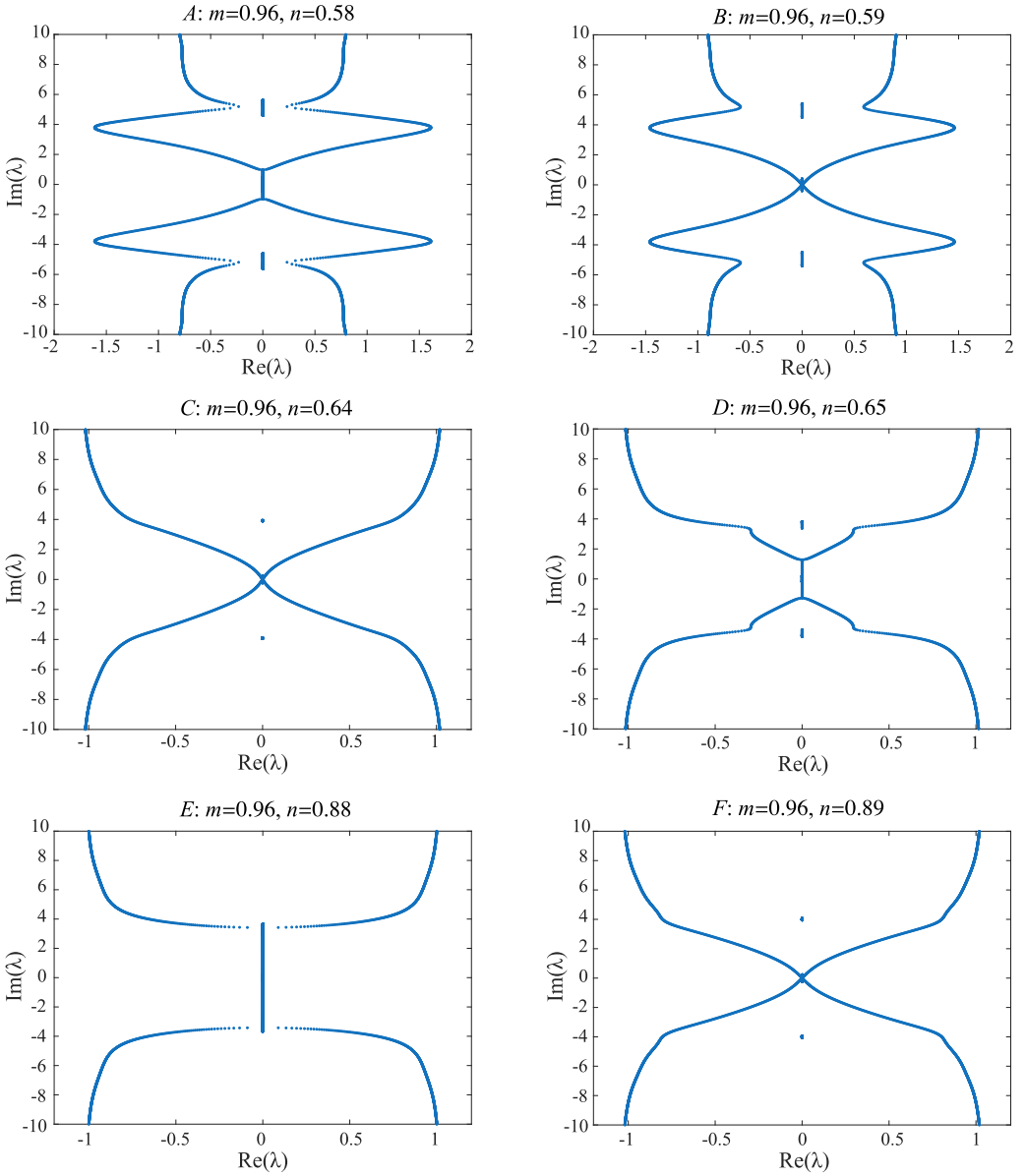


Figure 11. *Spectra of the linear operator at the parameter values marked by points A-F in Fig. 10.*

just outside and just inside the grey region, respectively. The corresponding spectra are shown in the two middle panels of Figure 8. Eigenvalues away from the imaginary axis correspond to instabilities. One can see that both solutions exhibit short-wavelength instabilities ($|\lambda| > 1$, $\mathrm{Re}(\lambda) \neq 0$), including superharmonic instabilities, studied in detail in [2], which are associated with the spectrum tending to infinity along vertical asymptotes. Note, however, the spectrum at A does not exhibit modulational instability (long wavelength, $\lambda \sim 0$ with nonzero real part), while the characteristic cross pattern of the spectrum near the origin associated with modulational instability is clearly seen at B, the point just inside the grey region. A similar emergence of modulational instability can be seen as we transition from point C just outside the grey region to the point D just inside it, as illustrated by the bottom panels in Fig. 8.

Downloaded from https://www.cambridge.org/core. 16 Nov 2026 at 15:29:29, subject to the Cambridge Core terms of use.

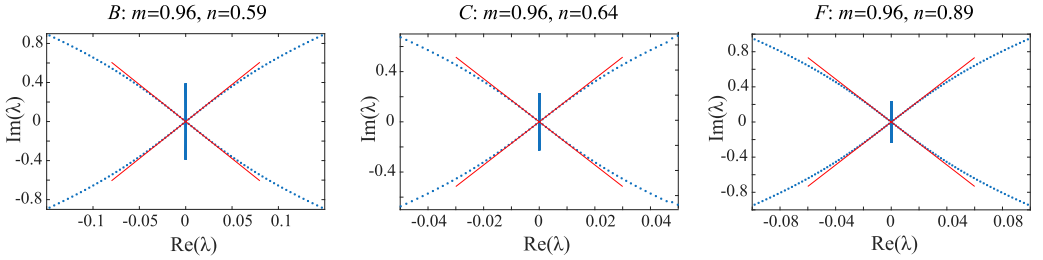


Figure 12. *Spectra of the linear operator at the parameter values marked by points B, C and F in Fig. 10 zoomed in around the origin, shown together with red straight lines obtained from the analysis of the Whitham system. See the text for details.*

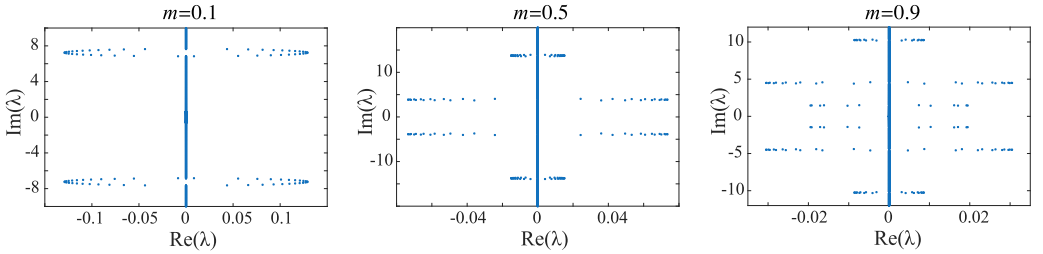


Figure 13. *Spectra of the linear operator at different values of parameter m for Case I with* $(\alpha, \beta) = (0, 1)$ *and real roots. Here* $a = 1$ *and* $n = 0.5$.

To see the dynamical consequences of modulational instability, we perturb the periodic travelling wave at $m = 0.886$, $a = 2.27$ (point B in the top panel of Fig. 8), the strain component of which is shown in Fig. 9(a), by adding the unstable mode associated with the eigenvalue $\lambda = 0.0019 + 0.0883i$ (shown in Fig. 9(b)), with the amplitude of perturbation $\varepsilon = 0.01$. The strain snapshot at $t = 8$ is shown in panel (c) of Fig. 9, with panels (d) and (e) zooming in on the top and left side of the strain profile, respectively. One can see that the strain profile clearly develops modulational instability of the same wavelength as the perturbation mode. Note, however, that in addition to this, a short-wavelength instability develops as well, as can be seen in panel (e), in agreement with the spectrum shown in the middle right panel of Figure 8 (point B). This instability is numerically found to eventually lead to the blowup of the solution.

To check the onset of modulational instability in the case $(\alpha, \beta) = (0, -1)$ (Case II), we consider the parameter values at points A-F in Fig. 10, which zooms in on the area in Fig. 7(d) (for periodic travelling waves of amplitude $a = 1.3$) near the tips of the grey regions where the Whitham system loses hyperbolicity. The corresponding spectra are shown in Fig. 11. One can see that the modulational instability develops as we transition from point A outside the lower grey region to point B inside it (top panels). Point C is still inside the region, and the corresponding spectrum (left middle panel of Figure 11) shows modulational instability. This instability disappears at point D (right middle panel), which is outside the grey region. The spectrum at point E, which is still in the domain of strict hyperbolicity (see Figure 10), is shown in the left lower panel of Fig. 11. One can see the modulational instability developing again at point E (right lower panel), which is just inside the top grey region in Figure 10. Note that in all cases there are short-wavelength instabilities.

When the spectrum exhibits modulational instability, one can see a characteristic cross structure near the origin. The slopes of this structure can be estimated using the complex-valued Whitham characteristic velocities σ and $\bar{\sigma}$ that lead to the instability. Indeed, for small wavenumber k we have $\mathrm{Re}(\lambda) \approx k\mathrm{Im}(\sigma)$ and $\mathrm{Im}(\lambda) \approx k(\mathrm{Re}(\sigma) - c)$, so that the slope $\mathrm{Im}(\lambda)/\mathrm{Re}(\lambda) \approx (\mathrm{Re}(\sigma) - c)/\mathrm{Im}(\sigma)$, and the same is true for $\bar{\sigma}$. To illustrate this, we show in Figure 12 the red lines with the corresponding

Downloaded from https://www.cambridge.org/core. 16 Nov 2026 at 15:29:29, subject to the Cambridge Core terms of use.

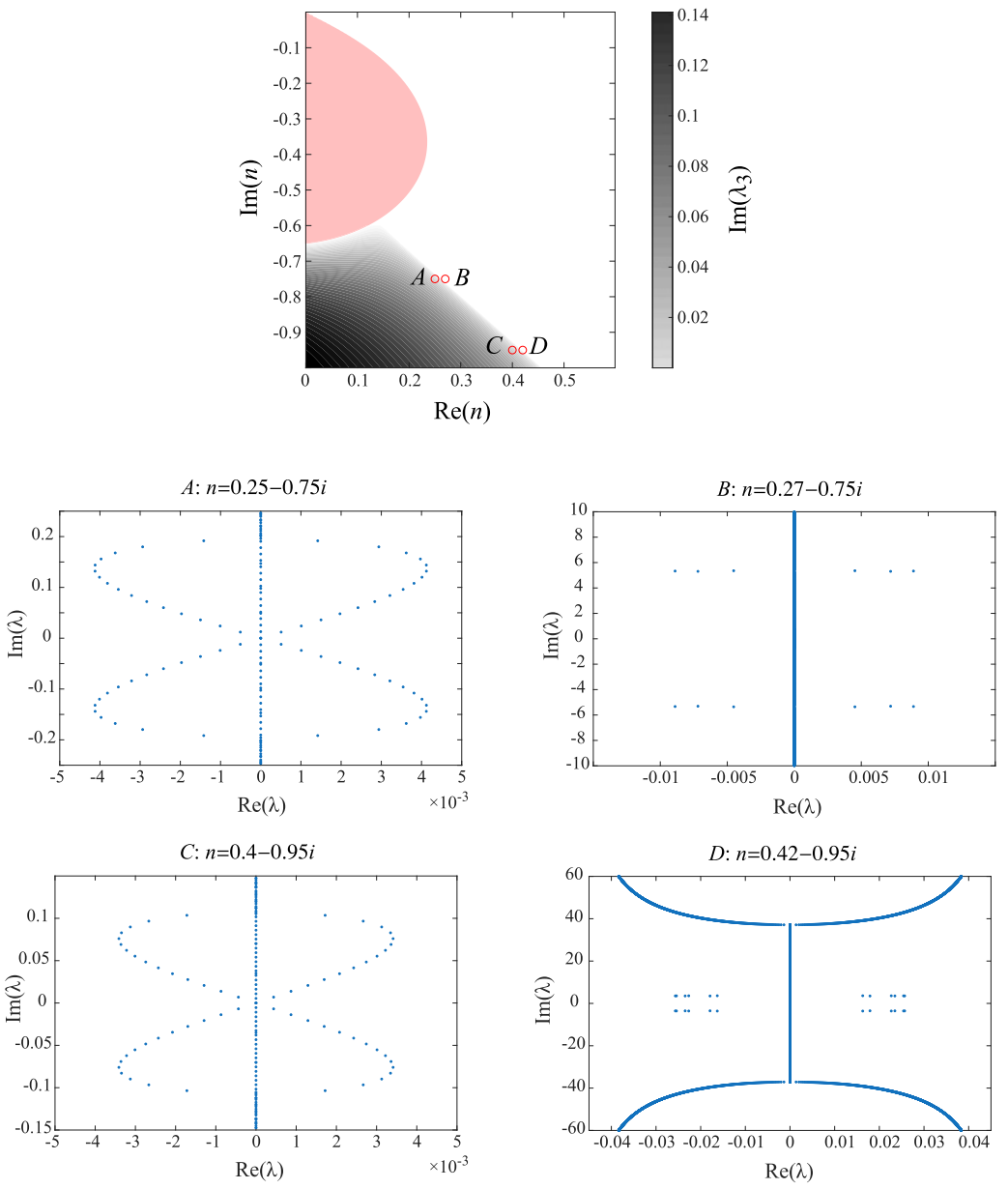


Figure 14. *Top panel: upper left part of a* $= 1$ *panel in Fig. 6 for Case I with* $(\alpha, \beta) = (0, 1)$*, real* $w_{1,2}$ *and complex* $w_{3,4}$*. Bottom panels: spectra of the linear operator at the parameter values marked by points A-D in the top panel.*

slopes superimposed with the spectra at the parameter values marked by points *B*, *C* and *F* in Fig. 10 zoomed in around the origin.

Finally, we consider Case I with $(\alpha, \beta) = (0, 1)$. Recall that in the case when all roots are real, no loss of hyperbolicity is observed, and thus all periodic travelling waves are expected to be modulationally stable (cf. Fig. 5). However, other instability modes are still present, as illustrated in Figure 13, where we use the transformation (3.35) to the parameter values (3.34). In the case when $w_{3,4}$ are complex, we found that the Whitham modulation equations are no longer hyperbolic

Downloaded from https://www.cambridge.org/core. 16 Nov 2026 at 15:29:29, subject to the Cambridge Core terms of use.

in certain parameter regimes as shown in Fig. 6. We use the transformation (3.39) to present the results in terms of (3.38) and recall that the existence region for the periodic travelling waves is given by (3.40). As shown in the top panel of Figure 14 (see also Figure 6 with $a = 1$), in this case there is a grey region associated with the loss of hyperbolicity and onset of modulational instability. This instability mode is evident in the spectra at points A and C just inside this region (left middle and bottom panels) and disappears in the spectra at points B and D just outside the grey region (right middle and bottom panels). However, the spectra at B and D feature short-wavelength instabilities.

Finally, we remark on the stability of the periodic solutions corresponding to the orbits shown in Fig. 1(a-c) and Fig. 2. All of these solutions are modulationally stable but exhibit instabilities of shorter wavelength, with the maximum of $|\mathrm{Re}\lambda|$ decreasing with amplitude for each set of orbits.

6. Concluding remarks

In this work, we derived the Whitham modulation equations for the modified regularized Boussinesq equation that approximates the FPU problem for cubic interaction force. We investigated the structure and convexity of the Whitham system in the case of generally nonconvex cubic nonlinearity, which yields explicit periodic travelling wave solutions and enables complete analysis of the exact solitary-wave, kink and harmonic limits. Away from these limits we conducted a systematic study of the system's convexity based on numerical computation of the eigenvalues and eigenvectors of the modulation matrix. Our results clarify how the regions where the system is convex depend on the amplitude, mean strain and other parameters of the periodic travelling waves.

We confirmed the onset of modulational instability due to the loss of hyperbolicity by computing the spectra of the linearized operator and conducting numerical simulations initiated by modulationally unstable waves perturbed along the corresponding eigenmode. Although we did not perform an exhaustive study of linear stability and mostly investigated solutions near the boundaries of the convexity region, our results show that both modulationally stable and unstable waves can exhibit short-wavelength instabilities that can lead to solution blowup, in agreement with earlier findings [2, 32]. These instabilities are not captured by the Whitham modulation system.

The results of this work pave the way for characterizing the jump conditions and the oscillatory structure of dispersive shock waves (DSWs) in the Boussinesq equation using the DSW fitting method [15], the analysis of exact solitary-wave limits [9] and the direct computation of the integral curves of the modulation system. The availability of the exact solitary-wave and harmonic-wave limits also enables a more precise analysis of the interactions between solitary waves or linear wavepackets and rarefaction waves or DSWs [9]. Future work will also include comparison of these results with simulations of FPU dynamics for cubic nonlinearity. In particular, it will be interesting to compare the regions of modulational and short-wavelength instabilities in the discrete problem and its quasicontinuum approximation.

Acknowledgements. The authors would like to thank the Isaac Newton Institute for Mathematical Sciences, Cambridge, for support and hospitality during the programme 'Emergent phenomena in nonlinear dispersive waves', where work on this paper was initiated.

Funding statement. This work was supported by EPSRC grant EP/V521929/1 and by grants DMS-2306319 (M.A.H.) and DMS-2204880 (A.V.) from the U.S. National Science Foundation.

Competing interests. The authors declare none.

References

[1] **Benzoni-Gavage S, Noble P and Rodrigues LM** (2014) Slow modulations of periodic waves in Hamiltonian PDEs, with application to capillary fluids. *Journal of Nonlinear Science* **24**(4), 711–768.

Downloaded from https://www.cambridge.org/core. 16 Nov 2026 at 15:29:29, subject to the Cambridge Core terms of use.

[2] **Bronski JC, Hur VM and Wester SL** (2023) Superharmonic instability for regularized long-wave models. *Nonlinearity* **36**(1), 133–170.

[3] **Bronski JC and Johnson MA** (2010) The modulational instability for a generalized Korteweg–de Vries equation. *Archive for Rational Mechanics and Analysis* **197**(2), 357–400.

[4] **Byrd PF and Friedman MD** (2013) *Handbook of Elliptic Integrals for Engineers and Physicists*, vol. **67**. Berlin, Heidelberg: Springer.

[5] **Chicone CC** (1999) *Ordinary Differential Equations With Applications.* New York: Springer.

[6] **Chong C, Herrmann M and Kevrekidis PG** (2022) Dispersive shock waves in lattices: A dimension reduction approach. *Physica D: Nonlinear Phenomena* **442**, 133533.

[7] **Chong C and Kevrekidis PG** (2018) *Coherent Structures in Granular crystals: From Experiment and Modelling to Computation and Mathematical analysis.* Heidelberg, New York: Springer.

[8] **Clarke WA, Marangell R and Perkins WR** (2022) Rigorous justification of the Whitham modulation equations for equations of Whitham type. *Studies in Applied Mathematics* **149**(2), 297–323.

[9] **Congy T, El GA, Gavrilyuk S, Hoefer MA and Shyue K-M** (2025) Solitary wave-mean flow interaction in strongly nonlinear dispersive shallow water waves. *Journal of Nonlinear Waves* **1**, e5.

[10] **Deconinck B and Kutz JN** (2006) Computing spectra of linear operators using the Floquet–Fourier–Hill method. *Journal of Computational Physics* **219**(1), 296–321.

[11] **Dreyer W and Herrmann M** (2008) Numerical experiments on the modulation theory for the nonlinear atomic chain. *Physica D: Nonlinear Phenomena* **237**(2), 255–282.

[12] **Dreyer W, Herrmann M and Mielke A** (2005) Micro–macro transition in the atomic chain via Whitham's modulation equation. *Nonlinearity* **19**(2), 471.

[13] **Dreyer W, M Herrmann and JDM Rademacher** (2006) Wave trains, solitons and modulation theory in FPU chains. In *Analysis, Modeling and Simulation of Multiscale Problems*. Berlin, Heidelberg: Springer, pp. 467–500.

[14] **Dubrovin BA and Novikov SP** (1989) Hydrodynamics of weakly deformed soliton lattices. Differential geometry and Hamiltonian theory. *Russian Mathematical Surveys* **44**(6), 35–124.

[15] **El GA** (2005) Resolution of a shock in hyperbolic systems modified by weak dispersion. *Chaos* **15**(3), 037103.

[16] **El GA and Hoefer MA** (2016) Dispersive shock waves and modulation theory. *Physica D: Nonlinear Phenomena* **333**, 11–65.

[17] **El GA, Hoefer MA and Shearer M** (2017) Dispersive and diffusive-dispersive shock waves for nonconvex conservation laws. *SIAM Review* **59**(1), 3–61.

[18] **Fermi, E., Pasta J, Ulam S** (1955). Studies of nonlinear problems. Technical report, I, Los Alamos Scientific Laboratory Report No. LA-1940.

[19] **Filip A and Venakides S** (1999) Existence and modulation of traveling waves in particle chains. *Communications on Pure and Applied Mathematics* **51**(6), 693–735.

[20] **Flach S and Gorbach AV** (2008) Discrete breathers — Advances in theory and applications. *Physics Reports* **467**(1), 1–116.

[21] **Gavrilyuk S, Nkonga B, Shyue K-M and Truskinovsky L** (2020) Stationary shock-like transition fronts in dispersive systems. *Nonlinearity* **33**(10), 5477.

[22] **Gorbushin N, Vainchtein A and Truskinovsky L** (2022) Transition fronts and their universality classes. *Physical Review E* **106**(2), 024210.

[23] **Herrmann M and Rademacher JDM** (2010) Riemann solvers and undercompressive shocks of convex FPU chains. *Nonlinearity* **23**(2), 277–304.

[24] **Johnson MA and Perkins WR** (2020) Modulational instability of viscous fluid conduit periodic waves. *SIAM Journal on Mathematical Analysis* **52**, 277–305.

[25] **Kamchatnov AM** (2000) *Nonlinear Periodic Waves and Their modulations: an Introductory course.* Singapore and River Edge, NJ: World Scientific.

[26] **Kamchatnov AM, Kuo Y-H, Lin T-C, Horng T-L, Gou S-C, Clift R, El GA and Grimshaw RHJ** (2012) Undular bore theory for the Gardner equation. *Physical Review E* **86**(3), 036605.

[27] **Kevrekidis PG** (2011) Non-linear waves in lattices: Past, present, future. *IMA Journal of Applied Mathematics* **76**(3), 1–35.

[28] **Kiper A** (1984) Fourier series coefficients for powers of the Jacobian elliptic functions. *Mathematics of Computation* **43**(167), 247–259.

[29] **Lax PD** (1973) *Hyperbolic Systems of Conservation Laws and the Mathematical Theory of Shock Waves.* Philadelphia, PA: SIAM.

[30] **Levermore C** (1988) The hyperbolic nature of the zero dispersion KdV limit. *Communications in Partial Differential Equations* **13**(4), 495–514.

[31] **Pankov A** (2005) *Travelling Waves and Periodic Oscillations in Fermi–Pasta–Ulam lattices.* London, UK: Imperial College Press.

[32] **Pava JA, Banquet C, Silva JD and Oliveira F** (2013) The regularized Boussinesq equation: instability of periodic traveling waves. *Journal of Differential Equations* **254**(9), 3994–4023.

[33] **Rosenau P** (1986) Dynamics of nonlinear mass-spring chains near the continuum limit. *Physics Letters A* **118**(5), 222–227.

[34] **Sen S, Hong J, Bang J, Avalos E and Doney R** (2008) Solitary waves in the granular chain. *Physics Reports* **462**(2), 21–66.

Downloaded from https://www.cambridge.org/core. 16 Nov 2026 at 15:29:29, subject to the Cambridge Core terms of use.

[35] **Sprenger P, Chong C, Okyere E, Herrmann M, Kevrekidis PG and Hoefer MA** (2024) Hydrodynamics of a discrete conservation law. *Studies in Applied Mathematics* **153**(4), e12767.
[36] **Vainchtein A and Truskinovsky L** (2024) When discrete fronts and pulses form a single family: FPU chain with hardening-softening springs. *Physica D: Nonlinear Phenomena* **464**, 134187.
[37] **Vainchtein A** (2020) Rarefactive lattice solitary waves with high-energy sonic limit. *Physical Review E* **102**(5), 052218.
[38] **Vainchtein A** (2022) Solitary waves in FPU–type lattices. *Physica D: Nonlinear Phenomena* **434**, 133252.
[39] **Whitham GB** (1999) *Linear and Nonlinear Waves.* New York: Wiley.
[40] **Yang S, Biondini G, Chong C and Kevrekidis PG** (2025) A regularized continuum model for traveling waves and dispersive shocks of the granular chain. *Journal of Nonlinear Waves* **1**, e2.

Cite this article: Hoefer MA and Vainchtein A (2026) Whitham modulation equations for the regularized Boussinesq equation with cubic nonlinearity. *Journal of Nonlinear Waves*, 1–42. https://doi.org/10.1017/jnw.2026.10042

Downloaded from https://www.cambridge.org/core. 16 Nov 2026 at 15:29:29, subject to the Cambridge Core terms of use.